INFLAMMATION–INDUCED DOWNREGULATION OF SUCCINATE DEHYDROGENASE REGULATES ADRENOCORTICAL FUNCTION

Ivona Mateska[1]*, Anke Witt[1], Eman Hagag[1], Anupam Sinha[1], Canelif Yilmaz[1], Evangelia Thanou[2], Na Sun[3], Ourania Kolliniati[4], Maria Patschin[1], Heba Abdelmegeed[1], Holger Henneicke[5,6], Waldemar Kanczkowski[1], Ben Wielockx[1], Christos Tsatsanis[4], Andreas Dahl[7], Axel Walch[3], Ka Wan Li[2], Mirko Peitzsch[1], Triantafyllos Chavakis[1], Vasileia Ismini Alexaki[1]*

[1] Institute of Clinical Chemistry and Laboratory Medicine, University Hospital, Technische Universität Dresden, Germany
[2] Center of Neurogenomics and Cognitive Research (CNCR), Department of Molecular and Cellular Neurobiology, Vrije Universiteit, Amsterdam, Netherlands
[3] Research Unit Analytical Pathology, German Research Center for Environmental Health, Helmholtz Zentrum München, Munich, Germany
[4] Department of Clinical Chemistry, Medical School, University of Crete, Heraklion, Greece
[5] Center for Regenerative Therapies, TU Dresden, Technische Universität Dresden, Germany
[6] Department of Medicine III & Center for Healthy Ageing, Technische Universität Dresden, Germany
[7] DRESDEN-concept Genome Center, Center for Molecular and Cellular Bioengineering, Technische Universität Dresden, Germany

*__Correspondence__:
Dr. V.I. Alexaki, Institute for Clinical Chemistry and Laboratory Medicine, University Hospital, Technische Universität Dresden, Fetscherstrasse 74, 01307 Dresden, Germany; +49 351 458 16273; VasileiaIsmini.Alexaki@uniklinikum-dresden.de
Dr. I. Mateska, Institute for Clinical Chemistry and Laboratory Medicine, University Hospital, Technische Universität Dresden, Fetscherstrasse 74, 01307 Dresden, Germany, Ivona.Mateska@uniklinikum-dresden.de

Running title: IL1β-induced adrenocortical metabolic rewiring

Keywords: adrenal gland / lipopolysaccharide (LPS) / IL1β / succinate / glucocorticoids

Abstract

The hypothalamus-pituitary-adrenal (HPA) axis is activated in response to inflammation leading to increased production of glucocorticoids by the adrenal cortex. In turn, glucocorticoids exert potent anti-inflammatory effects. Severe inflammation may reduce adrenal gland responsiveness to adrenocorticotropic hormone (ACTH) although the underlying molecular mechanisms are poorly understood. Here, we show by transcriptomic, proteomics and metabolomics analysis that lipopolysaccharide (LPS)-induced systemic inflammation triggers profound metabolic changes in steroidogenic adrenocortical cells, including downregulation of the tricarboxylic acid (TCA) cycle and oxidative phosphorylation, decreased ATP production and induction of oxidative stress. We demonstrate that although inflammation disrupts the TCA cycle at the levels of succinate dehydrogenase (SDH) and isocitrate dehydrogenase 2 (IDH2) leading to accumulation of succinate and isocitrate, respectively, only reduced SDH activity and increased succinate levels associate with disturbed steroidogenic capacity of adrenocortical cells. Specifically, IL1β reduces *Sdhb* expression and steroidogenesis in adrenocortical cells. These findings suggest that SDH activity is important for adrenocortical steroidogenesis and provide a link between inflammation and adrenocortical dysfunction through alterations in the TCA cycle.

Introduction

Stress triggers the hypothalamic–pituitary–adrenal (HPA) axis, i.e. the release of corticotropin-releasing hormone (CRH) from the hypothalamus, followed by adrenocorticotropic hormone (ACTH) secretion from the anterior pituitary, which stimulates the synthesis of glucocorticoid hormones in the adrenal cortex, primarily cortisol in humans and corticosterone in rodents (Chrousos, 1995; Lightman et al., 2021; Payne and Hales, 2004). Glucocorticoids are synthesized in the *zona fasciculata* of the adrenal cortex through sequential reactions (Midzak and Papadopoulos, 2016). The first step involves the transfer of cholesterol from the outer to the inner mitochondrial membrane, mediated by steroidogenic acute regulatory protein (StAR), followed by the CYP11A1 (P450scc)-mediated side-chain cleavage reaction producing pregnenolone (Midzak and Papadopoulos, 2016). Pregnenolone is then converted to progesterone through the NAD^+-dependent action of 3β-hydroxysteroid dehydrogenase (3β-HSD) (Midzak and Papadopoulos, 2016). CYP21 catalyzes the NADPH-dependent hydroxylation of progesterone and 17a-hydroxyprogesterone to 11-deoxycorticosterone and 11-deoxycortisol, respectively (Midzak and Papadopoulos, 2016). In the final step, CYP11B1 catalyzes the conversion of 11-deoxycortisol to cortisol in humans and 11-deoxycorticosterone to corticosterone in mice (Lightman et al., 2021; Midzak and Papadopoulos, 2016).

Glucocorticoids play a cardinal role in modifying the inflammatory response (Alexaki and Henneicke, 2021; Chrousos, 1995). Adrenalectomized rodents show increased mortality after induction of systemic inflammation, while glucocorticoid administration increases survival (Bertini *et al.*, 1988; Butler *et al.*, 1989). Similarly to any other stress stimulus, systemic inflammation activates the HPA axis leading to increased glucocorticoid release, which is required to restrain inflammation (Alexaki, 2021; Kanczkowski et al., 2013c, 2013a, 2013b). Adrenocortical cells were also reported to directly respond to inflammation. For instance, they express Toll like receptors (TLR), including TLR4 (Kanczkowski et al., 2009; Tran et al., 2007; Zacharowski et al., 2006). Treatment of mice with the TLR4 ligand lipopolysaccharide (LPS) induces leukocyte recruitment, apoptosis and transcriptional reprograming in the adrenal gland (Chen et al., 2020, 2019; Kanczkowski et al., 2013c; Tran et al., 2007). Essentially, severe

inflammation in sepsis is associated with impaired adrenal gland function (Annane et al., 2000; Boonen et al., 2015, 2014; Den Brinker et al., 2005; Jennewein et al., 2016). However, the mechanisms and particularly the cellular metabolic disturbances leading to adrenal gland dysfunction in systemic inflammation remain poorly understood.

In immune cells, such as macrophages, dendritic cells and T cells, inflammation triggers cellular metabolic reprograming, enabling the cells to meet the increased demands for fast energy supply and anabolic processes (Geltink et al., 2018; O'Neill and Pearce, 2016; Ryan and O'Neill, 2020). How inflammation may affect cellular metabolism in other cell types is less explored. Using systemic LPS-induced inflammation, we show that inflammation profoundly changes the cellular metabolism of adrenocortical cells. It perturbs tricarboxylic acid (TCA) cycle activity and oxidative phosphorylation and reduces ATP production in the adrenal cortex. These alterations, particularly succinate accumulation, can lead to reduced glucocorticoid production. Moreover, we show that particularly IL1β reduces SDHB expression and steroidogenesis. Hence, our data indicate regulation of adrenocortical steroidogenesis through TCA cycle modifications and provide a mechanistic explanation of adrenocortical dysfunction in severe inflammation.

Results

1. Inflammation reprograms cellular metabolism in the adrenal cortex.

To explore inflammation-induced alterations in the adrenal cortex, we performed RNA sequencing in microdissected adrenal cortices from mice treated for 6 hours via intraperitoneal (i.p.) injection with 1 mg / kg LPS or PBS. The RNA sequencing analysis revealed 2,609 differentially expressed genes, out of which 1,363 were down- and 1,246 were upregulated **(Figure 1A)**. Gene set enrichment analysis (GSEA) using the Molecular Signatures Database (MSigDB) hallmark gene set collection (Liberzon et al., 2015) showed a significant enrichment of inflammatory response-related gene sets in the adrenal cortex of LPS-treated mice **(Figure 1B)**. In acute inflammation, leukocytes infiltrate from blood vessels into the adrenal cortex (Kanczkowski et al., 2013c, 2013b). In addition, adrenal gland-resident immune cells, e.g.,

macrophages can be activated in response to LPS (González-Hernández et al., 1994; Schober et al., 1998). In order to delineate the inflammatory response between the different cell types comprising the adrenal cortex, we sorted $CD31^{-}CD45^{-}$, immune ($CD45^{+}$) and endothelial ($CD31^{+}$) cells from the adrenal cortex of PBS- and LPS-treated mice. The $CD31^{-}CD45^{-}$ cell population was enriched in steroidogenic adrenocortical cells as evidenced by high *Star* expression **(Supplementary Figure 1A)**, and its purity was verified by the absence of *Cd31* and *Cd45* expression **(Supplementary Figure 1B-C)**. Proteomic analysis in the sorted $CD31^{-}$ $CD45^{-}$ (steroidogenic) adrenocortical cell population from mice treated for 24 hours with LPS or PBS and GSE analysis of GO terms confirmed the enrichments of innate immune response-related proteins in adrenocortical cells of LPS-injected mice **(Figure 1C),** suggesting that steroidogenic adrenocortical cells respond to inflammatory stimuli.

LPS treatment leads to increased plasma corticosterone levels (Alexaki, 2021; Kanczkowski et al., 2013c, 2013b). Numerous studies have shown that elevated glucocorticoid levels are primarily driven by activation of the HPA axis, and coincide with increased circulating ACTH levels (Alexaki, 2021; Kanczkowski et al., 2013c, 2013b). This is accompanied by increased expression of genes related to steroid biosynthesis, as previously reported (Chen et al., 2019). We could confirm in our dataset an increased expression of the cholesterol transporter *Star* (Miller, 2007) and the terminal enzyme for glucocorticoids synthesis *Cyp11b1* (Payne and Hales, 2004) in adrenocortical cells of LPS-injected mice **(Supplementary Figure 2A-B)**. However, the expression of other steroidogenic enzymes, such as *3βHSD* and *Cyp21a1* was reduced, while *Cyp11a1* remained unchanged **(Supplementary Figure 2C-E)**. Similarly, protein levels of the transcription factor SF-1, a key regulator of adrenal steroidogenic function (Parker and Schimmer, 1997), were also somewhat reduced after LPS injection **(Supplementary Figure 2F-G)**. Therefore, the observed changes in plasma glucocorticoid levels which accompany inflammation cannot be solely explained by the transcriptional changes in the steroidogenic enzymes.

Next, we explored the cellular metabolic changes induced by LPS in the adrenal cortex. By GSEA of the RNA sequencing data we observed negative regulation of gene sets related to

carbohydrate and cellular metabolism in the adrenal cortex of LPS-injected mice **(Figure 1D)**. Proteomic analysis in sorted $CD31^{-}CD45^{-}$ adrenocortical cells of PBS- and LPS-treated mice was performed **(Supplementary Figure 1),** to examine specifically the effects of inflammation on the metabolism of steroidogenic adrenocortical cells, thus evading the well-described inflammation-induced metabolic changes in immune cells (O'Neill and Pearce, 2016; Ryan and O'Neill, 2020). Similarly to the RNA sequencing data, GSEA of the proteomic data using the Reactome Pathway Database showed significant negative enrichment of proteins associated with the carbohydrate metabolism in the steroidogenic adrenocortical cells **(Figure 1E).** EGSEA pathway analysis of the RNA sequencing and proteomic data revealed that TCA cycle, oxidative phosphorylation, tyrosine metabolism, fatty acid degradation, D-Glutamine and D-glutamate metabolism, glutathione metabolism and other metabolic pathways were significantly enriched among the downregulated genes and proteins in the adrenal cortex and in steroidogenic adrenocortical cells of LPS-treated mice **(Table 1 and Table 2)**.

2. Inflammation disrupts the TCA cycle in adrenocortical cells at the level of isocitrate dehydrogenase and succinate dehydrogenase.

Inflammation down-regulates the TCA cycle and oxidative phosphorylation in activated macrophages (Ryan and O'Neill, 2020), however little is known about inflammation-induced metabolic changes in other cell types. We started by investigating inflammation-induced TCA cycle alterations in adrenocortical cells and found that TCA cycle-related gene expression was downregulated in the adrenal cortex of LPS-treated mice **(Figure 2A-B, Table 1).** mRNA expression of genes encoding key TCA cycle enzymes, including succinate dehydrogenase subunits B and C (*Sdhb* and *Sdhc*), isocitrate dehydrogenase isoforms IDH2 and IDH3 (*Idh2* and *Idh3b*) and malate dehydrogenase 1 (*Mdh1*), was reduced in the adrenal cortex of LPS-injected mice **(Figure 2B)**. Proteomic GSEA analysis confirmed the downregulation of TCA cycle in steroidogenic adrenocortical cells of LPS-injected mice **(Figure 2C, Table 2).** Accordingly, $CD31^{-}CD45^{-}$ adrenocortical cells sorted from LPS-treated mice displayed reduced expression of the genes encoding cytoplasmic and mitochondrial isocitrate dehydrogenase

(*Idh1* and *Idh2,* respectively) (Yen et al., 2010) and succinate dehydrogenase (*Sdhb* and *Sdhc*) **(Figure 2D-E)**. Moreover, LPS treatment attenuated the IDH and SDH enzymatic activities in the isolated adrenal cortex **(Figure 2F-G)**. In endothelial cells and $CD45^+$ immune cells sorted from the adrenal cortex of LPS-injected mice, *Idh1* and *Idh2* gene expression was reduced, *Sdhb* gene expression was increased, while expression of *Sdhc* was unaltered **(Supplementary Figure 3A-B)**. Additionally, immunofluorescent staining in the adrenal gland showed that IDH2 and SDHB proteins are highly expressed in $SF\text{-}1^+$ steroidogenic cells **(Figure 2H-I)**. Collectively, these data indicate that the reduced activity of SDH and IDH in the adrenal cortex of LPS-treated mice is due to their downregulated expression and decreased activity in steroidogenic adrenocortical cells.

In order to confirm that inflammation disrupts the TCA cycle in adrenocortical cells, we profiled the changes in metabolite levels in the adrenal glands of PBS- and LPS-treated mice using liquid chromatography – tandem mass spectrometry (LC-MS/MS). The levels of citrate, cis-aconitate, isocitrate and succinate, as well as the ratios of isocitrate / α-ketoglutarate and succinate / fumarate were increased in the adrenal glands of LPS-treated mice **(Figure 2J-R)**. Furthermore, MS–Imaging confirmed the increased levels of isocitrate and succinate in the adrenal cortex of LPS-injected mice **(Figure 2S-T)**. These data suggest that LPS-induced inflammation disrupts IDH and SDH activity in adrenocortical cells.

3. Inflammation downregulates oxidative phosphorylation and increases oxidative stress in the adrenal cortex.

Next, we investigated how inflammation affects mitochondrial oxidative metabolism in adrenocortical cells. GSEA analysis of the RNA sequencing and proteomic data in the whole adrenal cortex and sorted $CD31^-CD45^-$ adrenocortical cells, respectively, revealed that oxidative phosphorylation was significantly enriched among the downregulated genes **(Figure 3A)** and translated proteins **(Figure 3B)**, and the expression of a large number of oxidative phosphorylation-associated genes was reduced in the adrenal cortex of LPS-treated mice **(Figure 3C)**. In accordance, ATP levels were reduced in the whole adrenal gland **(Figure 3D)**

and the mitochondrial membrane potential of $CD31^{-}CD45^{-}$ adrenocortical cells was decreased in mice treated with LPS **(Figure 3E)**. Collectively, these data suggest that inflammation disrupts mitochondrial function and ATP synthesis in the steroidogenic adrenocortical cells.

In pro-inflammatory macrophages, a TCA cycle 'break' at the level of SDH is associated with repurposing of mitochondria from oxidative phosphorylation-mediated ATP synthesis to ROS production (Mills et al., 2016). EGSEA pathway analysis showed that upon LPS treatment several pathways involved in the regulation of and the cellular response to oxidative stress in the adrenal cortex were enriched at mRNA **(Table 3)** and protein level **(Table 4).** This was confirmed by increased 4-hydroxynonenal (4-HNE) staining, indicating higher oxidative stress-associated damage in the adrenal cortex of LPS-treated mice **(Figure 3F-G)**. Antioxidant defense mechanisms are particularly important in the adrenal cortex, since electron leakage through the reactions catalyzed by CYP11A1 and CYP11B1 during glucocorticoid synthesis contributes significantly to mitochondrial ROS production (Prasad et al., 2014). Cells neutralize ROS to maintain their cellular redox environment by using the reducing equivalents NADPH and glutathione (Xiao and Loscalzo, 2020). In addition, in adrenocortical cells, NADPH serves as a co-factor for mitochondrial steroidogenic enzymes (Frederiks et al., 2007). We found that NADPH levels were significantly decreased in whole adrenal glands of LPS-treated mice **(Figure 3H)** and glutathione metabolism-related gene expression was downregulated in the inflamed adrenal cortex **(Figure 3I-J, Table 1, Table 2)**. These findings collectively suggest that inflammation in the adrenal cortex is associated with increased oxidative stress, perturbed mitochondrial oxidative metabolism, reduced anti-oxidant capacity and increased ROS production in the adrenal cortex.

4. Increased succinate levels impair mitochondrial metabolism and steroidogenesis in adrenocortical cells.

The TCA cycle produces NADH and $FADH_2$ for fueling the electron transfer chain (ETC) at the inner mitochondrial membrane (Martínez-Reyes et al., 2016). SDH is part of the ETC acting as complex II, coupling succinate oxidation in the TCA cycle with electron transfer along the

respiratory chain (Moosavi et al., 2020). Therefore, we tested if disturbing SDH activity would affect mitochondrial function. We inhibited SDH function with dimethyl malonate (DMM), which is hydrolyzed to the competitive SDH inhibitor malonate (Mills et al., 2016), or treated cells with the cell-permeable succinate analog diethyl succinate (DES). Both compounds increased the amount of succinate and the succinate / fumarate ratio in adrenal gland explants **(Figure 4A)** and in human adrenocortical carcinoma cells NCI-H295R (**Figure 4B).** Treatments with DMM and DES resulted in decreased mitochondrial oxygen consumption rate (OCR) and lower ATP production in NCI-H295R cells **(Figure 4C-D)**. The disturbed mitochondrial function in NCI-H295R cells was associated with reduction of mitochondrial membrane potential by DES **(Figure 4E)**, but not reduced mitochondrial load **(Figure 4F)**. Furthermore, DMM and DES increased ROS production in adrenocortical cells **(Figure 4G)**, suggesting that in adrenocortical cells, as in macrophages (Mills et al., 2016), succinate repurposes mitochondrial metabolism from oxidative phosphorylation to ROS production. In accordance with increased oxidative stress, SDH inhibition decreased NADPH levels in adrenocortical cells **(Figure 4H)**. Such changes in the mitochondrial function were not observed when inhibiting IDH activity with enasidenib (AG-221) (Yen et al., 2017) **(Figure 4I-K)**. AG-211 increased isocitrate and the isocitrate / α-ketoglutarate ratio **(Figure 4I)**, but did not affect OCR **(Figure 4J)** or the mitochondrial membrane potential **(Figure 4K).**

Key steps of steroidogenesis take place in mitochondria (Midzak and Papadopoulos, 2016), thus, we asked whether disruption of SDH activity affects adrenocortical steroidogenic function. To address this question, we inhibited SDH activity with DMM in human and mouse adrenocortical cells, and induced glucocorticoid production by forskolin or ACTH, respectively. SDH inhibition considerably impaired glucocorticoid and progesterone production in mouse primary adrenocortical cells **(Figure 5A-B),** adrenal gland explants **(Figure 5C-E)** and human adrenocortical NCI-H295R cells **(Supplementary Figure 4A-B)**. Similarly, DES diminished glucocorticoid production in mouse **(Figure 5A-B)** and human adrenocortical cells **(Supplementary Figure 4A-B).** Confirming these data, siRNA mediated *Sdhb* silencing (**Supplementary Figure 5A-B)**, impaired glucocorticoid synthesis in mouse primary

adrenocortical cells **(Figure 5F-H)** and NCI-H295R cells **(Supplementary Figure 4C)**, implying that proper adrenocortical steroidogenesis relies on intact SDH activity. Recently it was shown that SDH activity and intracellular succinate are required for CYP11A1-mediated pregnenolone synthesis, the first step of steroidogenesis (Bose et al., 2020). Our data confirm that physiological succinate concentrations support steroidogenesis, whereas treatment with increasing DES concentrations impairs ACTH-stimulated steroidogenesis in human adrenocortical cells **(Supplementary Figure 4D-F)**. Moreover, the proton gradient uncoupler FCCP **(Supplementary Figure 4G)** and the ATP synthase inhibitor oligomycin **(Figure 5I-K, Supplementary Figure 4H)** both abolished steroidogenesis in mouse **(Figure 5I-K)** and human adrenocortical cells **(Supplementary Figure 4G-H)**, demonstrating the previously reported requirement for intact mitochondrial membrane potential and ATP generation for steroidogenic function (Bose et al., 2020; King et al., 1999). In contrast, inhibition of IDH activity with enasidenib **(Figure 4I)**, did not alter glucocorticoid production in mouse adrenocortical cells **(Figure 5L-M)**, adrenal gland explants **(Figure 5N-O)** or human adrenocortical cells **(Supplementary Figure 4I-J),** nor did silencing of *Idh2* expression **(Supplementary Figure 5C)** in mouse primary adrenocortical cells **(Figure 5P-Q)**. Taken together, these results imply that disrupted SDH activity impairs oxidative mitochondrial metabolism and steroidogenesis in adrenocortical cells.

Gene expression analysis of steroidogenesis-related genes showed that inhibition of SDH activity with DMM or addition of DES downregulates the expression of the mitochondrial enzymes *Cyp11a1* and *Cyp11b1* **(Figure 5R-S)**. Both, CYP11A1 and CYP11B1 play critical roles in glucocorticoid synthesis, catalyzing the conversion of cholesterol to pregnenolone and the final step of cortisol/corticosterone production, respectively (Midzak and Papadopoulos, 2016; Payne and Hales, 2004). Reduced expression levels of these steroidogenic enzymes upon SDH inhibition could account at least in part for the reduced glucocorticoid production. Lastly, we wanted to confirm if disrupting SDH activity in the adrenal cortex upon inflammation could negatively affect adrenocortical steroidogenesis. Indeed, treatment of adrenal gland explants with LPS for 24 hours, similarly to SDH inhibition, reduced corticosterone secretion in response to ACTH stimulation **(Figure 5T)**.

5. IL1β downregulates SDHB expression and steroidogenesis.

Systemic inflammation in mice induces substantial leukocyte recruitment in the adrenal gland, accompanied by elevated production of pro-inflammatory cytokines (Chen et al., 2020; Kanczkowski et al., 2013c). IL-1β is highly produced by inflammatory monocytes and macrophages (Netea et al., 2010). RNA sequencing in the adrenal cortex, including recruited immune cells, showed increased expression of *Il1β* in LPS-injected mice compared to PBS controls (log2fc = 1.46, padj = 0.019). Furthermore, GSEA analysis using the GO database showed significant positive enrichment of genes associated with IL1β secretion in the adrenal cortex of mice treated with LPS **(Figure 6A).** The IL1β receptor *Il1r1* is expressed in $CD31^-$ $CD45^-$ adrenocortical cells and its expression was upregulated in adrenocortical cells sorted from LPS treated mice **(Figure 6B)**. In accordance, GSEA analysis showed positive enrichment of proteins related to IL1β signaling in $CD31^-CD45^-$ adrenocortical cells of mice treated with LPS **(Figure 6C)**. Hence, we asked whether IL1β can mediate the effect of inflammation on SDH expression and steroid synthesis in adrenocortical cells. Indeed, treatment of NCI-H295R cells with human recombinant IL1β, but not human recombinant IL6 or TNFα, reduced *SDHB* expression **(Figure 6D).** Moreover, treatment of primary adrenocortical cells with mouse recombinant IL1β protein impaired ACTH-induced steroid hormone production **(Figure 6E-G)**, suggesting that repression of SDH expression by IL1β results in accumulation of succinate, disturbed mitochondrial oxidative metabolism and impaired steroidogenesis in adrenocortical cells.

6. Itaconate is not responsible for reduced SDH activity and steroidogenesis in adrenocortical cells

It is known that the function of SDH in inflammatory macrophages can be inhibited by itaconate (Lampropoulou et al., 2016), a byproduct of the TCA cycle produced from cis-aconitate in a reaction catalyzed by aconitate decarboxylase 1 (ACOD1) (Michelucci et al., 2013). Expression of *Irg1*, the gene encoding for ACOD1, and itaconate are strongly upregulated in macrophages upon inflammation (Lampropoulou et al., 2016). *Irg1* expression was

upregulated in the adrenal cortex of LPS-treated mice but this increase derived from $CD45^+$ cells, while *Irg1* was not expressed in $CD31^-CD45^-$ (steroidogenic) adrenocortical cells **(Supplementary Figure 6A)**. Accordingly, LPS treatment significantly elevated itaconate levels in the $CD31^+CD45^+$ fraction, while it did not increase itaconate levels in sorted $CD31^-CD45^-$ adrenocortical cells **(Supplementary Figure 6B-C)**. Itaconate can be secreted from LPS-stimulated macrophages (Lampropoulou et al., 2016) and thereby it could affect SDH activity and associated steroidogenesis in adrenocortical cells. Hence, we tested whether exogenously given itaconate may affect steroidogenesis by treating primary mouse adrenocortical cells with the cell permeable itaconate derivative 4-octyl itaconate (4-OI). Adrenocortical cells could internalize the added itaconate derivative **(Supplementary Figure 6D)**, which however did not alter succinate levels, fumarate levels or the succinate / fumarate ratio **(Supplementary Figure 6E-G)**, nor did it affect glucocorticoid production **(Supplementary Figure 6H-I)**. Additionally, SDH activity in the adrenal cortex of *Irg1*-KO mice injected with LPS was not different from that in their wild-type counterparts **(Supplementary Figure 6J).** Hence, neither is itaconate produced in adrenocortical cells nor does it affect SDH activity of adrenocortical cells through paracrine routes.

Discussion

Glucocorticoid production in response to stress is essential for survival. The adrenal gland, the organ producing glucocorticoids, shows great resilience to damage induced by inflammation due to its strong regenerative capacity (Kanczkowski et al., 2013c; Lyraki and Schedl, 2021; Mateska et al., 2020). This maintains glucocorticoid release during infection or sterile inflammation, which is vital to restrain and resolve inflammation (Alexaki et al., 2018; Alexaki and Henneicke, 2021; Kourtzelis et al., 2020; Ziogas et al., 2020). However, severe sepsis is associated with adrenocortical impairment (Annane et al., 2006; Jennewein et al., 2016). We show that transcriptional and proteomic changes in the inflamed adrenal cortex reflect cellular metabolic reprograming which involves reduced TCA cycle, oxidative phosphorylation and glutathione metabolism, and increased oxidative stress. Succinate and isocitrate accumulate

due to decreased SDH and IDH expression and activity. Moreover, SDH but not IDH inhibition or silencing leads to reduced glucocorticoid synthesis in murine primary adrenocortical and NCI-H295R cells.

Our findings are in agreement with a recent report, which showed that SDH, i.e. complex II of the ETC, succinate and ATP are essential for CYP11A1 cleavage-mediated activation at the inner mitochondrial membrane, which is the rate-limiting step for pregnenolone synthesis (Bose et al., 2020). Although our data demonstrating reduced progesterone and glucocorticoid synthesis as a result of SDH inhibition are in line with these findings, we also found that DES at a high concentration (previously used in macrophages (Mills et al., 2016)) blunts steroidogenesis. We hypothesize that tightly regulated SDH activity and succinate are essential for normal steroidogenesis, while disturbed SDH function leading to succinate accumulation can disrupt steroidogenesis.

Pathogenic variants in *SDH* subunit genes leading to accumulation of succinate and increased succinate/fumarate ratio were described in neoplasms, including paragangliomas and pheochromocytomas (Richter et al., 2019, 2014). To our knowledge, germline or somatic *SDH* mutations are thus far not associated with adrenocortical insufficiency. SDH couples the oxidation of succinate to fumarate with the ETC in a manner that regulates ROS formation (Hadrava Vanova et al., 2020). On one hand, SDH mediates ROS production through reverse electron transfer to complex I (Hadrava Vanova et al., 2020). On the other hand, SDH inhibition / loss or increased succinate levels lead to augmented ROS generation, as shown in tumors and macrophages (Guzy et al., 2008; Hadrava Vanova et al., 2020; Mills et al., 2016; Ralph et al., 2011; Selak et al., 2005). Moreover, reduced SDH activity is associated with greater inflammation and oxidative stress in the visceral compared to the less inflamed subcutaneous adipose tissue of obese subjects (Michailidou et al., 2022; Ngo et al., 2019). Similarly, we show that SDH silencing or inhibition in adrenocortical cells, as well as high concentration of succinate, lead to increased ROS levels at the expense of mitochondrial oxidative function and ATP production. Adrenocortical disorders such as triple A syndrome and familial glucocorticoid deficiency can be driven by increased oxidative stress in the adrenal cortex (Prasad et al., 2014). In fact, mutations in genes encoding for proteins conferring antioxidant protection were

implicated in the development of these adrenocortical deficiencies (Prasad et al., 2014). Hence, disturbed SDH function may be an important component of the pathophysiology of adrenocortical insufficiency, a notion, which merits further investigation.

In the steroidogenic adrenocortical cells, ROS greatly derive from P450 enzymes. CYP11A1 and especially CYP11B1 are important ROS producing enzymes in the mitochondria of adrenocortical cells (Prasad et al., 2014). Hence, enhanced glucocorticoid production during inflammation or stress strongly increases ROS generation. In order to cope with steroidogenesis-related ROS production, adrenocortical cells have developed potent antioxidant defense mechanisms, such as the NADPH-dependent glutathione system (Prasad et al., 2014). Mitochondrial NADPH levels are maintained by the proton pump nicotinamide nucleotide transhydrogenase (NNT) and mutations in the *NNT* gene are associated with familial glucocorticoid deficiency (Meimaridou et al., 2012). We show that glutathione metabolism and NADPH levels are downregulated upon inflammation, which is rather counter-intuitive due to the great anti-oxidant demands in inflammation. While reduction of these anti-oxidant mechanisms may simply reflect mitochondrial damage, it could also confer regulation of glucocorticoid synthesis (Prasad et al., 2014). Indeed, disturbance of anti-oxidant mechanisms interferes with steroidogenesis in the adrenal gland and other steroidogenic organs (Kil et al., 2012; Meimaridou et al., 2012; Prasad et al., 2014).

Inflammation involves leukocyte recruitment in tissues, including the adrenal gland (Kanczkowski et al., 2013c, 2013b). We show by proteomic and transcriptional analyses that the inflammatory response targets steroidogenic adrenocortical cells (Chen et al., 2020, 2019). The *Il1r1* is particularly highly expressed in steroidogenic adrenocortical cells and its expression is upregulated by LPS. IL1β, mainly deriving from recruited neutrophils and monocytes/macrophages (Netea et al., 2010), impacts TCA cycle function in adrenocortical cells by reducing *SDH* expression, thereby impairing glucocorticoid production. The molecular mechanisms regulating *SDH* gene expression merit further investigation. However, regulation of SDH activity in adrenocortical cells by endogenously produced or exogenous itaconate can be excluded. In conclusion, in the present work we reveal a novel link between inflammation-induced disruption of the TCA cycle and glucocorticoid synthesis in adrenocortical cells. This

knowledge can contribute to a better understanding of adrenocortical dysfunction in severe inflammation or adrenocortical deficiencies, but can be also applied to other steroidogenic organs, such as the gonads or the brain (Yilmaz et al., 2019).

Materials and Methods

Animal experiments

Eight to twelve-week-old male C57BL/6J were injected intraperitoneally (i.p.) with 1 mg/kg lipopolysaccharide (LPS-EB Ultrapure; InVivoGen) or PBS as a control, and sacrificed after 6 hours (for RNA sequencing and gene expression analyses) or 24 hours (for all other analyses). *Irg1*$^{-/-}$ and littermate control mice were injected with 3 mg/kg LPS and sacrificed after 16 hours. The adrenal glands were excised in ice-cold PBS + 0.5 % bovine serum albumin (BSA; Sigma-Aldrich), cleaned from the surrounding fat tissue and processed for further analysis. The animal experiments were approved by the Landesdirektion Sachsen Germany.

Laser capture microdissection of adrenal cortex

Adrenal glands frozen in liquid nitrogen were cut in 25 - 30 μm thick sections, mounted on polyethylene naphthalate (PEN) membrane slides (Zeiss), dehydrated in increasing concentrations of ice-cold ethanol (75 %, 95 %, 100 %) for 45 seconds each, and air-dried at room temperature. Laser Capture Microdissection (LCM) was performed with a Zeiss PALM MicroBeam LCM system. The adrenal cortex from 8 to 12 sections was microdissected and the tissue was collected on Adhesive Caps (Zeiss).

Bioinformatics analysis of RNA sequencing data

For transcriptome mapping, strand-specific paired-end sequencing libraries from total RNA were constructed using TruSeq stranded Total RNA kit (Illumina Inc). Sequencing was performed on an Illumina HiSeq3000 (1x75 basepairs). Low quality nucleotides were removed with the Illumina fastq filter (http://cancan.cshl.edu/labmembers/gordon/fastq_illumina_filter/) and reads were further subjected to adaptor trimming using cutadapt (Martin, 2011). Alignment

of the reads to the Mouse genome was done using STAR Aligner (Dobin et al., 2013) using the parameters: "--runMode alignReads --outSAMstrandField intronMotif --outSAMtype BAM SortedByCoordinate --readFilesCommand zcat". Mouse Genome version GRCm38 (release M12 GENCODE) was used for the alignment. The parameters: 'htseq-count -f bam -s reverse -m union -a 20', HTSeq-0.6.1p1 (Anders et al., 2015) were used to count the reads that map to the genes in the aligned sample files. The GTF file (gencode.vM12.annotation.gtf) used for read quantification was downloaded from Gencode (https://www.gencodegenes.org/mouse/release_M12.html). Gene centric differential expression analysis was performed using DESeq2_1.8.1 (Anders and Huber, 2010). The raw read counts for the genes across the samples were normalized using 'rlog' command of DESeq2 and subsequently these values were used to render a PCA plot using ggplot2_1.0.1 (Wickham, 2009).

Pathway and functional analyses were performed using GSEA (Subramanian et al., 2005) and EGSEA (Alhamdoosh et al., 2017). GSEA is a stand-alone software with a GUI. To run GSEA, a ranked list of all the genes from DESeq2 based calculations was created by taking the -log10 of the p-value and multiplying it with the sign the of the fold change. This ranked list was then queried against Molecular Signatures Database (MSigDB), Reactome, KEGG and GO based repositories. EGSEA is an R/Bioconductor based command-line package. For doing functional analyses using EGSEA a differentially expressed list of genes with parameters log2foldchange > 0.3 and padj < 0.05 was used. Same database repositories as above were used for performing the functional analyses.

For constructing pathway-specific heatmaps, the "rlog-normalized" expression values of the significantly expressed genes (padj < 0.05) were mapped on to the KEGG and GO pathways. These pathway-specific expression matrices were then scaled using z-transformation. The resulting matrices were visually rendered using MORPHEUS.

Sorting of cell populations from the adrenal cortex

The adrenal cortex was separated from the medulla under a dissecting microscope and was digested in 1.6 mg/ml collagenase I (Sigma-Aldrich) and 1.6 mg/ml BSA in PBS, for 25 minutes

at 37 °C while shaking at 900 rpm. The dissociated tissue was passed through a 22 G needle and 100 μm cell strainer and centrifuged at 300 g for 5 minutes at 4 °C. The cell suspension was washed in MACS buffer (0.5 % BSA, 2 mM EDTA in PBS) and endothelial cells ($CD31^+$) and immune cells ($CD45^+$) were sequentially positively selected using anti-CD31 and anti-CD45 MicroBeads (Miltenyi Biotec), respectively, according to manufacturer's instructions. Briefly, pelleted cells resuspended in 190 μl MACS buffer, were mixed with 10 μl CD31 MicroBeads, incubated for 15 minutes at 4 °C, washed with 2 ml MACS buffer and centrifuged at 300 g for 10 minutes at 4 °C. Then, the cell pellet was resuspended in 500 μl MACS buffer, applied onto MS Column placed on MACS Separator, and the flow-through ($CD31^-$ cells) was collected. $CD31^+$ cells were positively sorted from the MS Columns. The flow-through was centrifuged at 300 g for 5 minutes at 4 °C, and the pelleted cells were subjected to the same procedure using CD45 MicroBeads, collecting the flow-through containing $CD31^-CD45^-$ adrenocortical cells. $CD45^+$ cells were positively sorted from the MS Columns.

MS/MS Proteomic analysis

Adrenocortical cells from 12 animals were sorted as $CD31^-CD45^-$ cells in PBS + 0.5% BSA + 2mM EDTA, as described above, and washed twice with PBS before snap-freezing in liquid nitrogen, until used. Samples were randomized and the gel-based sample preparation protocol was followed (Chen et al., 2011). In brief, the sorted cell pellets were resuspended in SDS loading buffer and 30% acrylamide, boiled at 98 °C for six minutes, and 5 μg protein per sample was separated in 10% SDS gels (SurePAGE Bis-Tris gels, GenScript) for approximately 10 minutes at 120 V. The gels were fixed in 50 % (v/v) ethanol and 3 % (v/v) phosphoric acid and briefly stained with Colloidal Coomassie Blue. Sample containing lanes were sliced and cut into blocks of approximately 1 mm^3, destained in 50 mM NH_4HCO_3 and 50 % (v/v) acetonitrile, dehydrated using 100 % acetonitrile, and rehydrated in 50 mM NH_4HCO_3 containing 10 μg / ml trypsin (sequence grade; Promega). After incubation overnight at 37 °C peptides were extracted and collected in a new tube, dried using a SpeedVac (Eppendorf), and stored at - 20 °C until LC-MS analysis. Peptides were redissolved in 0.1 % formic acid, and 75 ng were

loaded into EvoTips (EV2003, EvoSep) and washed according to manufacturer's guidelines. The samples were run on a 15 cm x 75 μm, 1.9 μm Performance Column (EV1112, EvoSep) using the Evosep one liquid chromatography system with the 30 samples per day program. Peptides were analyzed by the TimsTof pro2 mass spectrometer (Bruker) with the diaPASEF method (Meier et al., 2020). Data were analyzed using DIA-NN. The fasta database used was uniport mouse_UP000000589_10090. Deep learning was used to generate the in silico spectral library. Output was filtered at 0.01 FDR (Demichev et al., 2020). The Mass Spectrometry Downstream Analysis Pipeline (MS-DAP) (version beta 0.2.5.1) (https://github.com/ftwkoopmans/msdap) was used for quality control and candidate discovery (Hondius et al., 2021). Differential abundance analysis between groups was performed on log transformed protein abundances. Empirical Bayes moderated t-statistics with multiple testing correction by False Discovery Rate (FDR), as implemented by the eBayes functions from the limma R package, was used as was previously described (Koopmans et al., 2018).

Bioinformatics analysis of proteomics data

From the proteomics data, the missing data was imputed using the "impute" command running of "DEP" (Zhang et al., 2018) package in R/Bioconductor (Team, 2021) environment. The imputation was performed using "knn" function. The resultant imputed matrix was used for further analyses.

Pathway and functional analyses were performed using GSEA (Subramanian et al., 2005) and EGSEA (Alhamdoosh et al., 2017). CLI version of GSEA v4.1 was run using the imputed matrix. Different pathway sets from Molecular Signatures Database (MsigDB) v7.2 like, HALLMARK, Biocarta, Reactome, KEGG, GO and WIKIPATHWAYS were queried for functional enrichment. Geneset permutations were performed 1000 times to calculate the different statistical parameters. EGSEA is an R/Bioconductor based command-line package. For doing functional analyses using EGSEA, imputed matrix was used. Same database repositories as above were used for performing the functional analyses.

Quantitative RT - PCR

Total RNA was isolated from frozen adrenal glands with the TRI Reagent (MRC) after mechanical tissue disruption, extracted with chloroform and the NucleoSpin RNA Mini kit (Macherey-Nagel). Total RNA from sorted cells was isolated with the RNeasy Plus Micro Kit (Qiagen) according to manufacturer's instructions. cDNA was synthesized with the iScript cDNA Synthesis kit (Biorad) and gene expression was determined using the SsoFast Eva Green Supermix (Bio-Rad), with a CFX384 real-time System C1000 Thermal Cycler (Bio-Rad) and the Bio-Rad CFX Manager 3.1 software. The relative gene expression was calculated using the ΔΔCt method, *18S* was used as a reference gene. Primers are listed in **Table 5.**

Cell culture and in vitro treatments

For primary mouse adrenocortical cell culture, sorted adrenocortical cells were plated on 0.2 % gelatin-coated wells of a 96-well plate in DMEM/F12 medium supplemented with 1 % fetal bovine serum (FBS), 50 U/mL penicillin and 50 μg/mL streptomycin (all from Gibco), and let to attach for an hour before treatments. Cells from both adrenal glands from each mouse were pooled together and plated in 2 wells of a 96-well plate.

Mouse adrenal explants were dissected from surrounding fat and left in DMEM/F12 medium with 1 % FBS, 50 U/mL penicillin and 50 μg/mL streptomycin for an hour before treatments.

NCI-H295R cells were maintained in DMEM/F12 medium supplemented with 2.5 % Nu-Serum type I (Corning), 1 % Insulin Transferrin Selenium (ITS; Gibco), 50 U/mL penicillin and 50 μg/mL streptomycin.

Cells or explants were treated with DMM (20 mM; Sigma-Aldrich), DES (5 mM; Sigma-Aldrich), FCCP (1 μM; Agilent Technologies), OM (500 nM; Agilent Technologies), AG-221 (10 μM; Selleckchem), 4-OI (125 μM; Cayman Chemical), IL1β (20 ng/ml, PeproTech), IL6 (20 ng/ml, PeproTech), TNFα (20 ng/ml, PeproTech), LPS (1 μg/ml; InVivoGen), ACTH (100 ng/ml; Sigma-Aldrich) or Forskolin (10 μM; Sigma-Aldrich). siRNA transfection was done with ON-TARGETplus SMARTpool siRNA against human *SDHB* (10 nM), mouse *Sdhb* (30 nM) or

mouse *Idh2* (30 nM) (all from Horizon Discovery), with Lipofectamine RNAiMAX transfection reagent (Invitrogen), using a reverse transfection protocol per manufacturer's instructions. Supernatants were collected for steroid hormone measurement and cell or explant lysates were used for all the other metabolomic analyses or qPCR.

Steroid hormone measurement

Steroid hormones were analyzed by liquid chromatography tandem mass spectrometry (LC-MS/MS) in cell culture or explant supernatants as described previously (Peitzsch et al., 2015). Fifty to hundred μL cell culture supernatants were extracted by solid phase extraction using positive pressure, followed by a dry-down under gentle stream of nitrogen. Residues were reconstituted in 100 μL of the initial LC mobile phase and 10 μL were injected for detection by the triple quadrupole mass spectrometer in multiple reaction-monitoring scan mode using positive atmospheric pressure chemical ionization. Quantification of steroid concentrations was done by comparisons of ratios of analyte peak areas to respective peak areas of stable isotope labeled internal standards obtained in samples to those of calibrators.

Measurement of TCA cycle metabolites

TCA cycle metabolites were determined by liquid chromatography tandem mass spectrometry (LC-MS/MS) as described before (Richter et al., 2019). Itaconate was included in the existing LC-MS/MS method using multi-reaction monitoring (MRM)-derived ion transition of 128.9->85.1. For quantification of itaconate ratios of analyte peak areas to respective peak areas of the stable isotope labeled internal standard (itaconic acid-^{13}C5; Bio-Connect B.V., The Netherlands; MRM transition 133.9->89.1) obtained in samples were compared to those of calibrators.

MALDI-FT-ICR-MSI

Tissue preparation steps for MALDI imaging mass spectrometry (MALDI-MSI) analysis was performed as previously described (Aichler et al., 2017; Sun et al., 2018). Frozen mouse

adrenals were cryosectioned at 12 μm (CM1950, Leica Microsystems, Wetzlar, Germany) and thaw mounted onto indium-tin-oxide coated conductive slides (Bruker Daltonik, Bremen, Germany). The matrix solution consisted of 10 mg/ml 1,5-Diaminonaphthalene (Sigma-Aldrich, Germany) in water/acetonitril 30:70 (v/v). SunCollectTM automatic sprayer (Sunchrom, Friedrichsdorf, Germany) was used for matrix application. The MALDI-MSI measurement was performed on a Bruker Solarix 7T FT-ICR-MS (Bruker Daltonik, Bremen, Germany) in negative ion mode using 100 laser shots at a frequency of 1000 Hz. The MALDI-MSI data were acquired over a mass range of m/z 75-250 with 50 µm lateral resolution. Following the MALDI imaging experiments, the tissue sections were stained with hematoxylin and eosin (H&E) and scanned with an AxioScan.Z1 digital slide scanner (Zeiss, Jena, Germany) equipped with a 20x magnification objective. After the MALDI-MSI measurement, the acquired data underwent spectra processing in FlexImaging v. 5.0 (Bruker Daltonik, Bremen, Germany) and SCiLS Lab v. 2021 (Bruker Daltonik, Bremen, Germany). The mass spectra were root-mean-square normalized. MS Peak intensity of isocitrate and succinate of adrenal cortex regions were exported and applied for relative quantification analysis.

ATP measurement

Total ATP was measured in adrenal glands using the ATP Assay Kit (ab83355, Abcam) according to the manufacturer's instructions. Briefly, adrenal glands were collected, washed with PBS and immediately homogenized in 100 μl ATP assay buffer. Samples were cleared using the Deproteinizing Sample Preparation Kit - TCA (ab204708, Abcam). Samples were incubated for 30 minutes with the ATP reaction mix and fluorescence (Ex / Em = 535 / 587 nm) was measured using the Synergy HT microplate reader. The recorded measurements were normalized to the weight of the adrenal gland.

Reactive oxygen species measurement

ROS was detected using the DCFDA/H2DCFDA Cellular Reactive Oxygen Species Detection Assay Kit (ab113851, Abcam), according to manufacturer’s instructions. NCI-H295R cells

were plated at 80,000 cells / well in 96-well plate with black walls and clear bottom (Corning) and were incubated with 20 μM DCFDA Solution for 45 minutes at 37 °C in dark. Fluorescence (Ex / Em = 485 / 535 nm) was measured using the Synergy HT microplate reader.

ADP / ATP ratio measurement

Intracellular ATP / ADP ratio was determined with the ADP / ATP Ratio Assay Kit (MAK135, Sigma-Aldrich), according to manufacturer's instructions. NCI-H295R cells were plated at 80,000 cells / well in 96-well plate with white flat bottom wells (Corning). Luminescence was measured using the Synergy HT microplate reader.

NADP/NADPH measurement

Intracellular NADP/NADPH ratio was measured with the NADP/NADPH Assay Kit (Fluorometric) (ab176724, Abcam), according to manufacturer's instructions. NCI-H295R cells were plated at $5x10^6$ cells / 10 cm - diameter dish. Fluorescence (Ex / Em = 540 / 590 nm) was measured using the Synergy HT microplate reader. NADPH in adrenal tissue homogenates were analyzed by LC-MS/MS using an adapted method previously described (Yuan et al., 2012).

Enzyme activity measurement

SDH and IDH activities were measured using the Succinate Dehydrogenase Activity Colorimetric Assay Kit (MAK197, Sigma-Aldrich) or the Isocitrate Dehydrogenase Colorimetric Assay Kit (ab102528, Abcam), respectively, according to manufacturer's instructions. The adrenal cortex was dissected from the medulla and cortices from both adrenal glands of each mouse were pooled and processed together. Absorbance (at 600 nm for SDH or 450 nm for IDH) was detected using the Synergy HT microplate reader.

Seahorse assay

OCR measurements were performed with a Seahorse XF96 Analyzer (Agilent Technologies). NCI-H295R cells were plated at 80,000 cells / well in 0.2 % gelatin-precoated XF96 cell culture microplate (Agilent). The experimental medium used was XF Base Medium supplemented with glucose (10 mM), pyruvate (1 mM) and glutamine (2 mM).

Measurement of mitochondrial load and mitochondrial membrane potential

For measuring mitochondrial membrane potential in primary adrenocortical cells, the adrenal cortex was dissected from the medulla and digested in 1.6 mg/ml collagenase I and 1.6 mg/ml BSA in PBS, for 25 minutes at 37 °C while shaking at 900 rpm. After passing through a 22 G needle and 100 μm cell strainer, dissociated cells were centrifuged at 300 g for 5 minutes at 4 °C. Pelleted cells were resuspended in FACS buffer (0.5 % BSA, 2 mM EDTA in PBS) and incubated with Mitotracker Green (0.25 μM; Invitrogen), TMRE (2.5 μM; Thermofisher), CD31-PeCy7 (1:100; eBioscience) and CD45-PeCy7 (1:100; eBioscience) for 30 minutes at 37°C in dark. Live cells were selected by Hoechst staining. For measuring mitochondrial load and mitochondrial membrane potential in NCI-H295R cells, cells were plated at 250,000 cells / well in 24-well plates and treated with DES (5 mM) or AG-221 (10 μM) for 4 hours. After trypsinization, cells were collected in FACS buffer and incubated with MitotrackerGreen (100 nM) and TMRE (100 nM) for 30 minutes at 37 °C in dark. FACS was performed using a LSR Fortessa X20 flow cytometer and data were analyzed with the FlowJo software.

Western blotting

Cells were lysed with 10 mM Tris-HCl, pH7.4 + 1 % SDS + 1 mM sodium vanadate, cell lysates were centrifuged at 16,000 g for 5 minutes at 4 °C, cell supernatants were collected and total protein concentration was measured using Pierce BCA Protein Assay Kit (Thermo Scientific). Gel electrophoresis was performed according to standard protocols (Laemelli, 1970). Protein samples were prepared with 5x Reducing Laemmli buffer, denatured at 95 °C for 5 minutes and loaded on a 10 % acrylamide gel (Invitrogen) for sodium dodecyl sulfate polyacrylamide gel electrophoresis (SDS-PAGE). PageRuler Prestained Protein Ladder (Thermo Fisher

Scientific) were used as a protein size ladder. The separated proteins were transferred on Amersham Protran nitrocellulose membrane (GE Healthcare Lifescience). After blocking with 5 % skimmed milk in TBS-T (0.1 % Tween-20 (Sigma-Aldrich) in 1x Tris-buffered saline) for 1 hour at RT, membranes were incubated overnight at 4 °C with anti-SDHB (1:1000; Sigma-Aldrich, #HPA002868) and anti-Tubulin (1:3000; Sigma-Aldrich, T5186), diluted in 5 % BSA in TBS-T. After washing, membranes were incubated for 1 hour at RT with secondary antibodies: goat anti-rabbit IgG HRP- conjugated (1:3000; Jackson ImmunoResearch) or goat anti-mouse IgG HRP-conjugated (1:3000; Jackson ImmunoResearch), diluted in 5 % skimmed milk in TBS-T. The signal was detected using the Western Blot Ultra-Sensitive HRP Substrate (Takara) and imaged using the Fusion FX Imaging system (PeqLab Biotechnologie).

Immunofluorescent staining

Adrenal glands cleaned from surrounding fat tissue were fixed in 4 % PFA in PBS, washed overnight in PBS, cryopreserved in 30 % sucrose (AppliChem GmbH) in PBS overnight at 4°C, embedded in O.C.T. Compound (Tissue-Tek) and frozen at −80 °C. Each adrenal gland was cut into 8 μm thick serial sections. Before staining, adrenal sections were pre-warmed at RT for 30 minutes and antigen retrieval was performed by boiling in citrate buffer (pH 6) for 6 minutes. Adrenal sections were washed with PBS, permeabilized with 0.1 % Triton X-100 in PBS for 20 minutes, treated with TrueBlack Lipofuscin Quencher (1:40 in 70 % ethanol; Biotium) for 30 seconds to reduce autofluorescence and blocked for nonspecific binding in Dako Protein Block, serum-free buffer for 1 hour at RT. Then, sections were incubated overnight at 4 °C with primary antibodies, washed with PBS, and incubated for 1 hour at RT with the secondary antibodies together with DAPI (1:5,000; Roche), all diluted in Dako Antibody Diluent. Antibodies and dyes used were: anti-SDHB (1:300; Sigma-Aldrich, #HPA002868), anti-IDH2 (1:50; Sigma-Aldrich, #HPA007831), anti-SF-1 (1:100; TransGenic Inc. #KO610), Lectin Esculentum DyLight488 (1:300; Vector Laboratories, #DL-1174), 4-Hydroxynonenal (4-HNE, 1:200; Abcam, # ab48506), Alexa Fluor 555 donkey anti-rabbit (1:300; Life Technologies, #A-31572), Alexa Fluor 647 chicken anti-rat (1:300; Invitrogen,

#A21472) and Alexa Fluor 555 donkey anti-mouse (1:300; Invitrogen, #A31570). After washing with PBS, cryosections were mounted with Fluoromount (Sigma-Aldrich), covered with 0.17mm cover glass, fixed with nail polish and kept at 4 °C until imaging.

Image acquisition and image analysis

Z-series microscopic images for SDHB and IDH2 staining were acquired on Zeiss LSM 880 inverted confocal microscope (Zeiss, Jena, Germany), illuminated with laser lines at 405 nm, 488 nm, 561 nm and 633 nm, and detected by two photomultiplier tube detectors. EC Plan-Neofluoar objective with 40x magnification, 1.30 numerical aperture and M27 thread, working with an oil immersion medium Immersol 518 F, was used. Microscopic images of SF-1 and 4-HNE stainings were acquired with an Axio Observer Z1/7 inverted microscope with Apotome mode (Zeiss, Jena, Germany), illuminated with LED-Module 385 nm and 567 nm, on a Plan-Apochromat objective with 10x magnification, 0.45 numerical aperture and M27 thread. Laser power, photomultiplier gain and pinhole size were set for each antibody individually and kept constant for all image acquisitions. For each condition, at least 3 view-fields were imaged per tissue section. Images were acquired with the ZEN 3.2 blue edition software, and processed and quantified with the Fiji / ImageJ software on maximum intensity Z-projection images.

Statistical analysis

The statistical analysis and data plotting were done with the GraphPrism 7 software. The statistical tests used are described in each figure legend, $p < 0.05$ was set as a significance level, and data are represented as mean ± s.d.

Acknowledgements

We thank Christine Mund, Denise Kaden and Catleen Conrad for technical assistance. We acknowledge the technical support from the Core Facility Cellular Imaging of the Medical Faculty Carl Gustav Carus, TU Dresden for confocal imaging, and from the Light Microscopy Facility of the CMCB Technology Platform at TU Dresden, for laser microdissection. This work

was supported by grants from the Deutsche Forschungsgemeinschaft (SFB/TRR 205 to V.I. Alexaki, B. Wielockx and M. Peitzsch) and the European Union's Horizon 2020 research and innovation programme under the Marie Skłodowska-Curie grant agreement (No 765704 to V.I. Alexaki).

Author contributions

Ivona Mateska: Data curation, formal analysis, Investigation, Methodology, Validation, Visualization, Writing – original draft; **Anke Witt**: Data curation, Investigation; **Eman Hagag**: Data curation, Investigation; **Anupam Sinha**: Data curation, Validation; **Canelif Yilmaz**: Investigation, Methodology; **Evangelia Thanou**: Data curation, Investigation; **Na Sun**: Data curation, Investigation, Methodology; **Ourania Kolliniati**: Investigation; **Maria Patschin**: Investigation; **Heba Abdelmegeed**: Investigation; **Holger Henneicke**: Writing – review & editing; **Waldemar Kanczkowski**: Investigation, Methodology; **Ben Wielockx**: Writing – review & editing; **Christos Tsatsanis**: Validation, Resources; **Andreas Dahl**: Software, Methodology, Validation; **Axel Walch**: Methodology, Validation, Resources; **Ka Wan Li**: Methodology, Validation, Resources; **Mirko Peitzsch**: Methodology, Validation, Resources **Triantafyllos Chavakis**: Funding acquisition, Resources, Writing – review & editing; **Vasileia Ismini Alexaki**: Conceptualization, Data curation, Funding acquisition, Project Administraion, Resources, Supervision, Visualization, Writing – review & editing.

Conflict of interest

The authors declare that they have no conflict of interest.

References

Aichler M, Borgmann D, Krumsiek J, Buck A, MacDonald PE, Fox JEM, Lyon J, Light PE, Keipert S, Jastroch M *et al* (2017) N-acyl Taurines and Acylcarnitines Cause an Imbalance in Insulin Synthesis and Secretion Provoking β Cell Dysfunction in Type 2 Diabetes. *Cell Metab* 25: 1334-1347

Alexaki VI (2021) The Impact of Obesity on Microglial Function: Immune, Metabolic and Endocrine Perspectives. *Cells* 10(7):1584

Alexaki VI, Fodelianaki G, Neuwirth A, Mund C, Kourgiantaki A, Ieronimaki E, Lyroni K, Troullinaki M, Fujii C, Kanczkowski W *et al* (2018) DHEA inhibits acute microglia-mediated inflammation through activation of the TrkA-Akt1/2-CREB-Jmjd3 pathway. *Mol Psychiatry* 23: 1410–1420

Alexaki VI, Henneicke H (2021) The Role of Glucocorticoids in the Management of COVID-19. *Horm Metab Res* 53: 9–15

Alhamdoosh M, Ng M, Wilson NJ, Sheridan JM, Huynh H, Wilson MJ, Ritchie ME (2017) Combining multiple tools outperforms individual methods in gene set enrichment analyses. *Bioinformatics* 33: 414–424

Anders S, Huber W (2010) Differential expression analysis for sequence count data. *Genome Biol* 11: 4310–4315

Anders S, Pyl PT, Huber W (2015) HTSeq-A Python framework to work with high-throughput sequencing data. *Bioinformatics* 31: 166–169

Annane D, Maxime V, Ibrahim F, Alvarez JC, Abe E, Boudou P (2006) Diagnosis of adrenal insufficiency in severe sepsis and septic shock. *Am J Respir Crit Care Med* 174: 1319–1326

Annane D, Sébille V, Troché G, Raphaël JC, Gajdos P, Bellissant E (2000) A 3-level prognostic classification in septic shock based on cortisol levels and cortisol response to corticotropin. *J Am Med Assoc* 283: 1038–1045

Bertini R, Bianchi M, Ghezzi P (1988) Adrenalectomy sensitizes mice to the lethal effects of interleukin 1 and tumor necrosis factor. *J Exp Med* 167: 1708–1712

Boonen E, Bornstein SR, Van den Berghe G (2015) New insights into the controversy of adrenal function during critical illness. *Lancet Diabetes Endocrinol* 3: 805–815

Boonen E, Meersseman P, Vervenne H, Meyfroidt G, Guïza F, Wouters PJ, Veldhuis JD, Van den Berghe G (2014) Reduced nocturnal ACTH-driven cortisol secretion during critical illness. *Am J Physiol Endocrinol Metab* 306: 2–11

Bose HS, Marshall B, Debnath DK, Perry EW, Whittal RM (2020) Electron Transport Chain

Complex II Regulates Steroid Metabolism. *iScience* 23: 101295

Butler LD, Layman NK, Riedl PE, Cain RL, Shellhaas J, Evans GF, Zuckerman SH (1989) Neuroendocrine regulation of in vivo cytokine production and effects: I. In vivo regulatory networks involving the neuroendocrine system, interleukin-1 and tumor necrosis factor-α. *J Neuroimmunol* 24: 143–153

Chen LS, Singh SP, Müller G, Bornstein SR, Kanczkowski W (2020) Transcriptional Analysis of Sepsis-Induced Activation and Damage of the Adrenal Endothelial Microvascular Cells. *Front Endocrinol (Lausanne)* 10: 1–11

Chen LS, Singh SP, Schuster M, Grinenko T, Bornstein SR, Kanczkowski W (2019) RNA-seq analysis of LPS-induced transcriptional changes and its possible implications for the adrenal gland dysregulation during sepsis. *J Steroid Biochem Mol Biol* 191, 105360

Cheng N, Van Der Schors RC, Smit AB (2011) A 1D-PAGE/LC-ESI Linear Ion Trap Orbitrap MS Approach for the Analysis of Synapse Proteomes and Synaptic Protein Complexes, Neuroproteomics. *Humana Press*

Chrousos GP (1995) The hipothalamic-pituitary-adrenal axis and immune-mediated inflammation. *N Engl J Med* 332: 1351–1362

Demichev V, Messner CB, Vernardis SI, Lilley KS, Ralser M (2020) DIA-NN: neural networks and interference correction enable deep proteome coverage in high throughput. *Nat Methods* 17: 41–44

Den Brinker M, Joosten KFM, Liem O, De Jong FH, Hop WCJ, Hazelzet JA, Van Dijk M, Hokken-Koelega ACS (2005) Adrenal insufficiency in meningococcal sepsis: Bioavailable cortisol levels and impact of interleukin-6 levels and intubation with etomidate on adrenal function and mortality. *J Clin Endocrinol Metab* 90: 5110–5117

Dobin A, Davis CA, Schlesinger F, Drenkow J, Zaleski C, Jha S, Batut P, Chaisson M, Gingeras TR (2013) STAR: Ultrafast universal RNA-seq aligner. *Bioinformatics* 29: 15–21

Frederiks WM, Kümmerlin IPED, Bosch KS, Vreeling-Sindelarova H, Jonker A, Van Noorden, CJF (2007) NADPH production by the pentose phosphate pathway in the zona fasciculata of rat adrenal gland. *J Histochem Cytochem* 55: 975–980

Geltink RIK, Kyle RL, Pearce EL (2018) Unraveling the Complex Interplay between T Cell Metabolism and Function. *Annu Rev Immunol* 36: 461–488

González-Hernández JA, Bornstein SR, Ehrhart-Bornstein M, Geschwend JE, Adler G, Scherbaum WA (1994) Macrophages within the human adrenal gland. *Cell Tissue Res* 278: 201–205

Guzy RD, Sharma B, Bell E, Chandel NS, Schumacker PT (2008) Loss of the SdhB, but Not the SdhA, Subunit of Complex II Triggers Reactive Oxygen Species-Dependent Hypoxia-Inducible Factor Activation and Tumorigenesis. *Mol Cell Biol* 28: 718–731

Hadrava Vanova K, Kraus M, Neuzil J, Rohlena J (2020) Mitochondrial complex II and reactive oxygen species in disease and therapy. *Redox Rep* 25: 26–32

Hondius DC, Koopmans F, Leistner C, Pita-Illobre D, Peferoen-Baert RM, Marbus F, Paliukhovich I, Li KW, Rozemuller AJM, Hoozemans JJM, Smit AB (2021) The proteome of granulovacuolar degeneration and neurofibrillary tangles in Alzheimer's disease. *Acta Neuropathol* (141) 341–358

Jennewein C, Tran N, Kanczkowski W, Heerdegen L, Kantharajah A, Dröse S, Bornstein S, Scheller B, Zacharowski K (2016) Mortality of Septic Mice Strongly Correlates with Adrenal Gland Inflammation. *Crit Care Med* 44: e190–e199

Kanczkowski W, Alexaki VI, Tran N, Großklaus S, Zacharowski K, Martinez A, Popovics P, Block NL, Chavakis T, Schally AV, Bornstein SR (2013a) Hypothalamo-pituitary and immune-dependent adrenal regulation during systemic inflammation. *Proc Natl Acad Sci USA* 110: 14801–14806

Kanczkowski W, Chatzigeorgiou A, Grossklaus S, Sprott D, Bornstein SR, Chavakis T (2013b) Role of the endothelial-derived endogenous anti-inflammatory factor del-1 in inflammation-mediated adrenal gland dysfunction. *Endocrinology* 154: 1181–1189

Kanczkowski W, Chatzigeorgiou A, Samus M, Tran N, Zacharowski K, Chavakis T, Bornstein SR (2013c) Characterization of the LPS-induced inflammation of the adrenal gland in mice. *Mol Cell Endocrinol* 371: 228–235

Kanczkowski W, Zacharowski K, Wirth MP, Ehrhart-Bornstein M, Bornstein SR (2009) Differential expression and action of Toll-like receptors in human adrenocortical cells.

Mol Cell Endocrinol 300: 57–65

Kil IS, Lee SK, Ryu KW, Woo HA, Hu MC, Bae SH, Rhee SG (2012) Feedback Control of Adrenal Steroidogenesis via H2O2-Dependent, Reversible Inactivation of Peroxiredoxin III in Mitochondria. *Mol Cell* 46: 584–594

King SR, Liu Z, Soh J, Eimerl S, Orly J, Stocco DM (1999) Effects of disruption of the mitochondrial electrochemical gradient on steroidogenesis and the steroidogenic acute regulatory (StAR) protein. *J Steroid Biochem Mol Biol* 69: 143–154

Koopmans F, Pandya NJ, Franke SK, Phillippens IHCMH, Paliukhovich I, Li KW, Smit AB (2018) Comparative Hippocampal Synaptic Proteomes of Rodents and Primates: Differences in Neuroplasticity-Related Proteins. *Front Mol Neurosci* 11: 1–14

Kourtzelis I, Hajishengallis G, Chavakis T (2020). Phagocytosis of Apoptotic Cells in Resolution of Inflammation. *Front Immunol* 11: 1–8

Laemelli UK (1970) Cleavage of Structural Proteins during the Assembly of the Head of Bacteriophage T4. *Nature* 227: 680–685

Lampropoulou V, Sergushichev A, Bambouskova M, Nair S, Vincent EE, Loginicheva E, Cervantes-Barragan L, Ma X, Huang SCC, Griss T *et al* (2016) Itaconate Links Inhibition of Succinate Dehydrogenase with Macrophage Metabolic Remodeling and Regulation of Inflammation. *Cell Metab* 24: 158–166

Liberzon A, Birger C, Thorvaldsdóttir H, Ghandi M, Mesirov JP, Tamayo P (2015) The Molecular Signatures Database Hallmark Gene Set Collection. *Cell Syst* 1: 417–425

Lightman SL, Birnie MT, Conway-Campbell BL (2021) Dynamics of ACTH and cortisol secretion and implications for disease. *Endocr Rev* 41: 470–490

Lyraki R, Schedl A (2021) Adrenal cortex renewal in health and disease. *Nat Rev Endocrinol* 17: 421–434

Martin M (2011) Cutadept removes adapter sequences from high-throughput sequncing reads. *EMBnet.journal* 7: 2803–2809

Martínez-Reyes I, Diebold LP, Kong H, Schieber M, Huang H, Hensley CT, Mehta MM, Wang T, Santos JH, Woychik R *et al* (2016) TCA Cycle and Mitochondrial Membrane Potential Are Necessary for Diverse Biological Functions. *Mol Cell* 61: 199–209

Mateska I, Nanda K, Dye NA, Alexaki VI, Eaton S (2020) Range of SHH signaling in adrenal gland is limited by membrane contact to cells with primary cilia. *J Cell Biol* 219(12):e201910087

Meier F, Brunner AD, Frank M, Ha A, Bludau I, Voytik E, Kaspar-Schoenefeld S, Lubeck M, Raether O, Bache N, Aebersold R, Collins BC, Röst HL, Mann M (2020) diaPASEF: parallel accumulation–serial fragmentation combined with data-independent acquisition. *Nat Methods* 17: 1229–1236

Meimaridou E, Kowalczyk J, Guasti L, Hughes CR, Wagner F, Frommolt P, Nürnberg P, Mann NP, Banerjee R, Saka HN *et al* (2012) Mutations in NNT encoding nicotinamide nucleotide transhydrogenase cause familial glucocorticoid deficiency. *Nat Genet* 44: 740–2

Michailidou Z, Gomez-Salazar M, Alexaki VI (2022) Innate Immune Cells in the Adipose Tissue in Health and Metabolic Disease. *J Innate Immun* 14: 4–30

Michelucci A, Cordes T, Ghelfi J, Pailot A, Reiling N, Goldmann O, Binz T, Wegner A, Tallam A, Rausell A et al (2013) Immune-responsive gene 1 protein links metabolism to immunity by catalyzing itaconic acid production. *Proc Natl Acad Sci USA* 110: 7820–7825

Midzak A, Papadopoulos V (2016) Adrenal mitochondria and steroidogenesis: From individual proteins to functional protein assemblies. *Front Endocrinol (Lausanne)* 7: 1–14

Miller WL (2007) Steroidogenic acute regulatory protein (StAR), a novel mitochondrial cholesterol transporter. *Biochim Biophys Acta* 1771(6):663-76.

Mills EL, Kelly B, Logan A, Costa ASH, Varma M, Bryant CE, Tourlomousis P, Däbritz JHM, Gottlieb E, Latorre I *et al* (2016) Succinate Dehydrogenase Supports Metabolic Repurposing of Mitochondria to Drive Inflammatory Macrophages. *Cell* 167: 457-470

Moosavi B, Zhu XL, Yang WC, Yang GF (2020) Genetic, epigenetic and biochemical regulation of succinate dehydrogenase function. *Biol Chem* 401: 319–330

Netea MG, Simon A, Van De Veerdonk F, Kullberg BJ, Van Der Meer JWM, Joosten LAB (2010) IL-1β processing in host defense: Beyond the inflammasomes. *PLoS Pathog*

6(2):e1000661.

Ngo DTM, Sverdlov AL, Karki S, Macartney-Coxson D, Stubbs RS, Farb MG, Carmine B, Hess DT, Colucci WS, Gokce N (2019) Oxidative modifications of mitochondrial complex ii are associated with insulin resistance of visceral fat in obesity. *Am J Physiol Endocrinol Metab* 316: E168–E177.

O'Neill LAJ, Pearce EJ (2016) Immunometabolism governs dendritic cell and macrophage function. *J Exp Med* 213: 15–23.

Parker KL, Schimmer BP (1997) Steroidogenic factor 1: a key mediator of endocrine development and function. *Endocr Rev* 18: 361–377

Payne AH, Hales DB (2004) Overview of steroidogenic enzymes in the pathway from cholesterol to active steroid hormones. *Endocr Rev* 25: 947–70

Peitzsch M, Dekkers T, Haase M, Sweep FCGJ, Quack I, Antoch G, Siegert G, Lenders JW, Deinum J, Willenberg HS *et al* (2015) An LC-MS/MS method for steroid profiling during adrenal venous sampling for investigation of primary aldosteronism. *J Steroid Chem Mol Biol* 145, 75–84

Prasad R, Kowalczyk JC, Meimaridou E, Storr HL, Metherell LA (2014) Oxidative stress and adrenocortical insufficiency. *J Endocrinol* 221(3):R63-73

Ralph SJ, Moreno-Sánchez R, Neuzil J, Rodríguez-Enríquez S (2011) Inhibitors of succinate: Quinone reductase/Complex II regulate production of mitochondrial reactive oxygen species and protect normal cells from ischemic damage but induce specific cancer cell death. *Pharm Res* 28: 2695–2730

Richter S, Gieldon L, Pang Y, Peitzsch M, Huynh T, Leton R, Viana B, Ercolino T, Mangelis A, Rapizzi E *et al* (2019) Metabolome-guided genomics to identify pathogenic variants in isocitrate dehydrogenase, fumarate hydratase, and succinate dehydrogenase genes in pheochromocytoma and paraganglioma. *Genet Med* 21: 705–717

Richter S, Peitzsch M, Rapizzi E, Lenders JW, Qin N, De Cubas AA, Schiavi F, Rao JU, Beuschlein F, Quinkler M *et al* (2014) Krebs cycle metabolite profiling for identification and stratification of pheochromocytomas/paragangliomas due to succinate dehydrogenase deficiency. *J Clin Endocrinol Metab* 99: 3903–3911

Ryan DG, O'Neill LAJ (2020) Krebs Cycle Reborn in Macrophage Immunometabolism. *Annu Rev Immunol* 38: 289–313

Schober A, Huber K, Fey J, Unsicker K (1998) Distinct populations of macrophages in the adult rat adrenal gland: A subpopulation with neurotrophin-4-like immunoreactivity. *Cell Tissue Res* 291: 365–373

Selak MA, Armour SM, MacKenzie ED, Boulahbel H, Watson DG, Mansfield KD, Pan Y, Simon MC, Thompson CB, Gottlieb E (2005) Succinate links TCA cycle dysfunction to oncogenesis by inhibiting HIF-α prolyl hydroxylase. *Cancer Cell* 7: 77–85

Subramanian A, Tamayo P, Mootha VK, Mukherjee S, Ebert BL, Gillette MA, Paulovich A, Pomeroy SL, Golub TR, Lander ES *et al* (2005) Gene set enrichment analysis: A knowledge-based approach for interpreting genome-wide expression profiles. *Proc Natl Acad Sci USA* 102: 15545–15550

Sun N, Fernandez IE, Wei M, Witting M, Aichler M, Feuchtinger A, Burgstaller G, Verleden SE, Schmitt-Kopplin P, Eickelberg O *et al* (2018) Pharmacometabolic response to pirfenidone in pulmonary fibrosis detected by MALDI-FTICR-MSI. *Eur Respir J* 52: (3):1702314

Team RC (2021) R: A language and environment for statistical computing. R Foundation for Statistical Computing. Vienna, Austria.

Tran N, Koch A, Berkels R, Boehm O, Zacharowski PA, Baumgarten G, Knuefermann P, Schott M, Kanczkowski W, Bornstein SR *et al* (2007) Toll-like receptor 9 expression in murine and human adrenal glands and possible implications during inflammation. *J Clin Endocrinol Metab* 92: 2773–2783

Wickham H (2009). ggplot2: elegant graphics for data analysis. *Springer New York*

Xiao W, Loscalzo J (2020). Metabolic Responses to Reductive Stress. *Antioxidants Redox Signal* 32: 1330–1347

Yen K, Travins J, Wang F, David MD, Artin E, Straley K, Padyana A, Gross S, Delabarre B, Tobin E, *et al* (2017). AG-221, a first-in-class therapy targeting acute myeloid leukemia harboring oncogenic IDH2 mutations. *Cancer Discov* 7: 478–493

Yen KE, Bittinger MA, Su SM, Fantin VR (2010) Cancer-associated IDH mutations:

Biomarker and therapeutic opportunities. *Oncogene* 29: 6409–6417

Yilmaz C, Karali K, Fodelianaki G, Gravanis A, Chavakis T, Charalampopoulos I, Alexaki VI (2019) Neurosteroids as regulators of neuroinflammation. *Front.Neuroendocrinol* 55:100788.

Yuan M, Breitkopf SB, Yang X, Asara JM (2012) A positive/negative ion-switching, targeted mass spectrometry-based metabolomics platform for bodily fluids, cells, and fresh and fixed tissue. *Nat Protoc* 7: 872–881

Zacharowski K, Zacharowski PA, Koch A, Baban A, Tran N, Berkels R, Papewalis C, Schulze-Osthoff K, Knuefermann P, Zähringer U *et al* 2006. Toll-like receptor 4 plays a crucial role in the immune-adrenal response to systemic inflammatory response syndrome. *Proc Natl Acad Sci USA* 103: 6392–6397

Zhang X, Smits AH, Van Tilburg GBA, Ovaa H, Huber W, Vermeulen M (2018) Proteome-wide identification of ubiquitin interactions using UbIA-MS. *Nat Protoc* 13: 530–550

Ziogas A, Maekawa T, Wiessner JR, Le TT, Sprott D, Troullinaki M, Neuwirth A, Anastasopoulou V, Grossklaus S, Chung KJ *et al* (2020) DHEA Inhibits Leukocyte Recruitment through Regulation of the Integrin Antagonist DEL-1. *J Immunol* 204: 1214–1224

Figure legends

Figure 1. LPS-induced inflammation changes the transcriptional and proteomic profile of the adrenal cortex. A, Volcano plot showing differentially expressed genes in the microdissected adrenal gland cortex of mice treated for 6 hours with PBS or LPS. **B,** GSEA analysis for immune pathway genes in the adrenal cortex of LPS- compared to PBS-injected mice. **C,** GSEA analysis for proteins associated with the innate immune response in $CD31^-$ $CD45^-$ adrenocortical cells of mice treated for 24h with PBS or LPS. **D,** GSEA analysis for carbohydrate metabolism pathways genes in the adrenal cortex of LPS- compared to PBS-injected mice. **E,** GSEA analysis for proteins associated with carbohydrate metabolism in $CD31^-CD45^-$ adrenocortical cells of LPS- compared to PBS-injected mice. NES: normalized

enrichment score. **A,B,D:** n = 3 mice per group, **C,E:** n = 6 mice per group, padj < 0.05 was used as a cut-off for significance.

Figure 2. Systemic inflammation disrupts the TCA cycle in the adrenal cortex. A,B. Transcriptome analysis in the microdissected adrenal gland cortex of mice treated for 6 hours with PBS or LPS (n = 3 mice per group). **A,** GSEA for TCA cycle-associated genes. **B,** Heatmap of differentially expressed TCA cycle genes (padj < 0.05). **C,** GSEA analysis for TCA cycle-associated proteins in $CD31^{-}CD45^{-}$ adrenocortical cells of mice treated for 24h with PBS or LPS (n = 6 mice per group). **D,E,** mRNA expression of *Idh1*, *Idh2*, *Sdhb* and *Sdhc* in adrenocortical $CD31^{-}CD45^{-}$ cells isolated from adrenal glands of mice 6 hours after injection of PBS or LPS (n = 8 mice per group, shown is one from two experiments). **F,G,** Quantification of IDH and SDH activities in the adrenal cortex of mice treated with LPS or PBS for 24 hours (n = 6 mice per group). Values are normalized to the total protein amount in the adrenal cortex. **H,I,** Immunofluorescence image of adrenal gland, stained for isocitrate dehydrogenase (IDH2, red) or succinate dehydrogenase (SDHB, red), Isolectin (endothelial cells, green), SF-1 (adrenocortical cells, magenta) and nuclear DAPI (blue). Scale bar, 30 μm. A zoomed-in insert of each image is included. **J-R,** TCA cycle metabolites (citrate, cis-aconitate, isocitrate, α-ketoglutarate, succinate, fumarate and malate) were measured by LC–MS/MS in adrenal glands of mice 24 hours after injection with PBS or LPS (n = 4 mice per group, shown is one from two experiments). **S-T,** MS-Imaging of isocitrate and succinate in the adrenal cortex of mice treated with PBS or LPS for 24 hours (n = 3 mice per group). Representative images and quantification are shown. Scale bar, 500 μm. Data are presented as mean ± s.d., p values were calculated with two-tailed Mann-Whitney test **(D-G, J-P)** or one-tailed Mann-Whitney test **(Q-T)**. *p < 0.05, **p < 0.01, ***p < 0.001, ****p < 0.0001.

Figure 3. Inflammation downregulates oxidative phosphorylation and increases oxidative stress in the adrenal cortex. A, GSEA for oxidative phosphorylation genes, RNASeq was performed in the microdissected adrenal cortex of mice treated for 6 hours with

PBS or LPS. **B,** GSEA analysis for TCA cycle-associated proteins in $CD31^-CD45^-$ adrenocortical cells of mice treated for 24h with PBS or LPS (n = 6 mice per group). **C,** Heatmap of differentially expressed oxidative phosphorylation genes (padj < 0.05). **D,** Measurement of ATP in adrenal glands of mice treated for 24 hours with PBS or LPS (n = 10-11 mice per group, pooled from two independent experiments). **E,** Measurement of mitochondrial membrane potential by TMRE staining and mitochondrial load by Mitotracker Green FM in adrenocortical ($CD31^-CD45^-$) cells isolated from mice injected with PBS or LPS. Flow cytometry was performed 24 hours post-injection, data are presented as ratio of the median fluorescence intensities of TMRE to Mitotracker Green (n = 6 mice per group). **F,** Representative immunofluorescence images of adrenal gland sections from PBS- and LPS-treated mice (24 hours post-injection), stained for 4-HNE (magenta) and nuclear DAPI (blue). Scale bar, 300 μm. **G,** Quantification of the mean fluorescence intensity of 4-HNE staining in the adrenal cortex of PBS- or LPS-treated mice (n = 6 mice per group). **H,** NADPH measurement by LC–MS/MS in adrenal glands of mice treated with PBS or LPS for 24 hours (n = 8 mice per group). Data are given as observed peak area intensities of NADPH. **I,** GSEA for glutathione metabolism genes, RNASeq was performed in the microdissected adrenal cortex of mice treated for 6 hours with PBS or LPS. **J,** Heatmap of differentially expressed glutathione metabolism genes (padj < 0.05). Data in **D,E,G,H** present mean ± s.d., p values were calculated with two-tailed Mann-Whitney test. *p < 0.05, **p < 0.01.

Figure 4. Disruption of succinate dehydrogenase function in adrenocortical cells impairs mitochondrial metabolism and function. A,B Succinate and fumarate levels were measured by LC–MS/MS in adrenal gland explants **(A)** and NCI-H295R cells **(B)** treated with dimethyl malonate (DMM, 20 mM) or diethyl succinate (DES, 5 mM) for 24 hours (n = 5 and n = 4 for **(A)** and **(B)**, respectively). **C,** Oxygen consumption rate (OCR) measurement with Seahorse technology in NCI-H295R cells treated with DMM (20 mM) or DES (5 mM) for 24 hours (n = 6). **D,** Measurement of ATP/ADP ratio in NCI-H295R cells treated with DMM (20 mM) or DES (5 mM) for 24 hours (n = 4-8). **E,F** Mitochondrial membrane potential (TMRE

staining) **(E)** and mitochondrial load (Mitotracker Green FM staining) **(F)** followed by flow cytometry in NCI-H295R cells treated with DES (5 mM) for 4 hours, mean fluorescence intensity is shown (n = 7 for **(E)** and n = 4, one from two experiments for **(F)**). **G,** ROS measurement in NCI-H295R cells treated with DMM (20 mM) or DES (5 mM) for 2 hours (n = 10 - 12). **H,** Measurement of NADPH/NADP ratio in NCI-H295R cells treated with DMM (20 mM) for 24 hours (n = 3 - 4). **I,** Isocitrate levels measured by LC–MS/MS in NCI-H295R cells treated with enasidenib (AG221, 10 μM) or DMSO as control for 24 hours (n = 6). **J,** OCR measurement in NCI-H295R cells treated with AG221 (10 μM) or DMSO for 24 hours. (n = 10). **K,** Measurement of mitochondrial membrane potential in NCI-H295R cells treated with AG221 (10 μM) or DMSO for 4 hours, by TMRE staining and flow cytometry, presented as mean fluorescence intensity (n = 7). Data in **A-B,D-H,I,K,** are presented as mean ± s.d., p values were calculated with one-way ANOVA **(A,D,G)** or two-tailed Mann-Whitney test **(B,E,F,H,I,K)**. Data in **C** and **J,** are shown as mean ± s.e.m. *p < 0.05, **p < 0.01, ***p < 0.001, ****p < 0.0001.

Figure 5. Disruption of succinate dehydrogenase function in adrenocortical cells impairs glucocorticoid production in the mouse adrenal cortex. A,B, Primary adrenocortical cells were treated with DMM (20 mM) or DES (5 mM) for 24 hours and ACTH (10 ng/mL) for another 45 minutes (n = 5-6). **C-E,** Adrenal gland explants were treated with DMM (20 mM) or DES (5 mM) for 24 hours and ACTH (100 ng/mL) for another 45 minutes (n = 5). **F-H,** Primary adrenocortical cells were transfected with siRNA against *Sdhb* (si*Sdhb*, 30 nM) or control siRNA (siCtrl) and 24 hours post-transfection treated with ACTH (10 ng/mL) for 45 minutes (n = 7-8). **I-K,** Primary adrenocortical cells were treated for 24 hours with oligomycin (500 nM) and for another 45 minutes with ACTH (10 ng/mL) (n = 6). **L-M,** Primary adrenocortical cells were treated for 24 hours with AG221 (10 μM) or DMSO and for another 45 minutes with ACTH (10 ng/mL) (n = 6). **N-O,** Adrenal gland explants were treated for 24 hours with AG221 (10 μM) or DMSO and for another 45 minutes with ACTH (100 ng/mL) (n = 4). **P-Q,** Primary adrenocortical cells were transfected with siRNA against *Idh2* (si*Idh2*, 30 nM) or control siRNA (siCtrl) and 24 hours post-transfection treated for 45 minutes with ACTH (10

ng/mL) (n = 7). **R-S,** mRNA expression of steroidogenic enzymes *Cyp11a1* and *Cyp11b1* in primary adrenocortical cell cultures treated for 24 hours with DMM (20 mM) or DES (5 mM) and then with ACTH (10 ng/mL) for 45 minutes (n = 5-6). **T,** Adrenal gland explants were treated for 24 hours with LPS (1 μg/mL) and for another 45 minutes ACTH (100 ng/mL) (n = 4-5). Measurements of steroid hormones in **A-Q** and **T,** were performed in supernatants of primary adrenocortical cell cultures or adrenal gland explants by LC-MS/MS. Data are shown as mean ± s.d., p values were calculated with one-way ANOVA. *p < 0.05, **p < 0.01, ***p < 0.001, ****p < 0.0001. BLD = below level of detection.

Figure 6. IL1β reduces glucocorticoid synthesis in adrenocortical cells. A, GSEA for genes related to positive regulation of IL1β secretion in the adrenal cortex of mice treated for 6 hours with PBS or LPS (n = 3 mice per group). **B,** mRNA expression of *Il1r1* in adrenocortical $CD31^{-}CD45^{-}$ cells isolated from adrenal cortices of mice 6 hours after injection of PBS or LPS (n = 6 mice per group). **C,** GSEA for proteins related to IL1β signaling in $CD31^{-}CD45^{-}$ adrenocortical cells isolated from mice treated for 24 hours with PBS or LPS (n = 6 mice per group). **D,** mRNA expression of *SDHB* in NCI-H295R cells treated for 2 hours with IL1β (20 ng/ml), IL6 (20 ng/ml) or TNFα (20 ng/ml) (n = 6). **E-G,** Primary adrenocortical cells were treated for 6 hours with IL1β (20 ng/ml) and for another 45 minutes with ACTH (10 ng/mL) (n = 11-12). Steroid hormones were measured in the culture supernatant by LC-MS/MS. Data in **B,D-G** are shown as mean ± s.d., p values were calculated with two-tailed Mann-Whitney test **(B,D)** or two-tailed Wilcoxon test **(E-G).** *p < 0.05, **p < 0.01.

Tables

Table 1. Cellular metabolic pathways transcriptionally regulated by inflammation in the adrenal cortex. The pathway analysis of differentially expressed genes was done with the software package EGSEA and queried against the KEGG Pathways repository. Pathways with p < 0.05 are shown.

ID	Metabolic pathway	Number of expressed genes	p value	p adj	avg.logfc	Direc-tion
mmu00190	Oxidative phosphorylation	132/134	8.32E-15	7.32E-13	0.613034377	Down
mmu00280	Valine, leucine and isoleucine degradation	55/56	1.16E-05	0.001119154	0.725758563	Down
mmu00511	Other glycan degradation	18/18	3.82E-05	0.001119154	0.29921956	Down
mmu00980	Metabolism of xenobiotics by cytochrome P450	65/65	0.000282456	0.006214029	0.650304677	Down
mmu00350	Tyrosine metabolism	38/39	0.001754788	0.030884268	0.305935415	Down
mmu00640	Propanoate metabolism	31/31	0.002151447	0.031554563	0.886410728	Down
mmu00020	Citrate cycle (TCA cycle)	32/32	0.003091828	0.034636464	0.21912487	Down
mmu01200	Carbon metabolism	118/118	0.003685749	0.034636464	0.715139933	Down
mmu00471	D-Glutamine and D-glutamate metabolism	3/3	0.003980826	0.034636464	0.338725016	Up
mmu00300	Lysine biosynthesis	2/2	0.004518807	0.034636464	0.156233777	Down
mmu00630	Glyoxylate and dicarboxylate metabolism	29/29	0.006079126	0.034636464	0.886410728	Down
mmu00071	Fatty acid degradation	49/49	0.006124673	0.034636464	0.401441917	Down
mmu01210	2-Oxocarboxylic acid metabolism	19/19	0.006297539	0.034636464	0.942661129	Down
mmu00920	Sulfur metabolism	11/11	0.006297539	0.034636464	0.601864913	Down
mmu00480	Glutathione metabolism	58/59	0.006297539	0.034636464	0.550257753	Down
mmu00510	N-Glycan biosynthesis	49/49	0.006297539	0.034636464	0.254426968	Down
mmu00450	Selenocompound metabolism	17/17	0.009115527	0.047186259	0.329118527	Up
mmu00514	Other types of O-glycan biosynthesis	22/22	0.010614958	0.050693394	0.204924928	Up
mmu00440	Phosphonate and phosphinate metabolism	6/6	0.010945165	0.050693394	0.291510253	Up
mmu00120	Primary bile acid biosynthesis	16/16	0.011193422	0.052510566	2.713591551	Down
mmu00565	Ether lipid metabolism	44/44	0.016711812	0.061724814	0.433837026	Down
mmu00520	Amino sugar and nucleotide sugar metabolism	49/49	0.018212661	0.061724814	0.652646241	Down
mmu00790	Folate biosynthesis	14/14	0.01821569	0.061724814	0.420000237	Down
mmu00230	Purine metabolism	174/178	0.018793387	0.061724814	0.830115541	Down
mmu00603	Glycosphingolipid biosynthesis - globo series	16/16	0.019832034	0.061724814	0.534287429	Up

mmu00534	Glycosaminoglycan biosynthesis - haparan sulfate/heparin	24/24	0.020491524	0.061724814	0.471378176	Up
mmu00270	Cysteine and methionine metabolism	46/48	0.020959507	0.061724814	0.601864913	Down
mmu01100	Metabolic pathways	1303/1315	0.022419002	0.061724814	0.683947211	Down
mmu00531	Glycosaminoglycan degradation	21/21	0.023139686	0.061724814	0.911753864	Down
mmu00604	Glycosphingolipid biosynthesis - ganglio series	15/15	0.023268716	0.061724814	0.457285673	Down
mmu00250	Alanine, aspartate and glutamate metabolism	36/37	0.023685519	0.061724814	0.942661129	Down
mmu00240	Pyrimidine metabolism	101/104	0.024235887	0.061724814	0.308135641	Up
mmu00130	Ubiquinone and other terpenoid-quinone biosynthesis	11/11	0.024630584	0.061724814	0.40991964	Down
mmu00330	Arginine and proline metabolism	49/50	0.025088792	0.061724814	0.479554867	Down
mmu00564	Glycerophospholipid metabolism	94/94	0.025448859	0.061724814	0.498146256	Down
mmu00910	Nitrogen metabolism	17/17	0.025782601	0.061724814	1.765582115	Up
mmu00982	Drug metabolism - cytochrome P450	67/67	0.027201304	0.061724814	0.620562175	Down
mmu00785	Lipoic acid metabolism	3/3	0.027507553	0.061724814	0.133403173	Down
mmu00051	Fructose and mannose metabolism	35/35	0.029679889	0.061724814	0.652646241	Down
mmu00561	Glycerolipid metabolism	59/59	0.030468773	0.061724814	0.4155946	Down
mmu00512	Mucin type O-glycan biosynthesis	28/28	0.030540327	0.061724814	0.472458211	Up
mmu00052	Galactose metabolism	32/32	0.031376559	0.061724814	0.42838689	Down
mmu01230	Biosynthesis of amino acids	78/78	0.031800904	0.061724814	0.942661129	Down
mmu00533	Glycosaminoglycan biosynthesis - keratan sulfate	14/14	0.031872109	0.061724814	0.27544313	Down
mmu00900	Terpenoid backbone biosynthesis	22/23	0.032232321	0.061724814	0.320850492	Up
mmu00730	Thiamine metabolism	15/15	0.032265244	0.061724814	0.323024942	Down
mmu00500	Starch and sucrose metabolism	33/33	0.033413545	0.062178073	0.452533726	Up
mmu00770	Pantothenate and CoA biosynthesis	18/18	0.033915312	0.062178073	0.307590054	Down
mmu00062	Fatty acid elongation	27/27	0.035703854	0.062200773	0.536297353	Down
mmu00592	alpha-Linolenic acid metabolism	25/25	0.035861114	0.062200773	0.568488547	Down
mmu00562	Inositol phosphate metabolism	70/70	0.037060597	0.062200773	0.197317479	Up

mmu00760	Nicotinate and nicotinamide metabolism	34/35	0.037777703	0.062200773	0.44361797	Down
mmu00740	Riboflavin metabolism	8/8	0.038531607	0.062200773	0.336638606	Down
mmu00670	One carbon pool by folate	19/19	0.039807001	0.062200773	0.293141874	Up
mmu00310	Lysine degradation	57/59	0.040221284	0.062200773	0.409052131	Up
mmu00010	Glycolysis / Gluconeogenesis	66/66	0.040372513	0.062200773	0.4474754	Down
mmu00053	Ascorbate and aldarate metabolism	27/27	0.040535303	0.062200773	0.319047565	Down
mmu00030	Pentose phosphate pathway	32/32	0.040995964	0.062200773	0.316347941	Down

Table 2. Cellular metabolic pathways regulated on protein level by inflammation in adrenocortical cells. The pathway analysis of differentially expressed proteins was done with the software package EGSEA and queried against the KEGG Pathways repository. Pathways with $p < 0.05$ are shown.

ID	Metabolic pathway	Number of detected proteins	p.value	p.adj	avg.logfc	Direction
mmu00534	Glycosaminoglycan biosynthesis - heparan sulfate / heparin	4/24	1.50E-07	1.29E-05	0.13	Up
mmu00280	Valine, leucine and isoleucine degradation	37/57	5.20E-07	2.23E-05	0.01	Down
mmu00983	Drug metabolism - other enzymes	25/92	3.80E-05	0.000856142	0.02	Down
mmu00562	Inositol phosphate metabolism	19/72	5.89E-05	0.000856142	0.03	Up
mmu00260	Glycine, serine and threonine metabolism	19/40	6.89E-05	0.000856142	0.03	Down
mmu00240	Pyrimidine metabolism	25/58	6.98E-05	0.000856142	0.04	Up
mmu00982	Drug metabolism - cytochrome P450	16/71	7.76E-05	0.000856142	0.02	Down
mmu00230	Purine metabolism	44/133	7.96E-05	0.000856142	0.04	Up
mmu00790	Folate biosynthesis	9/26	9.75E-05	0.000931452	0.09	Up
mmu01100	Metabolic pathways	593/1608	0.000134694	0.001151176	0.03	Down
mmu00190	Oxidative phosphorylation	70/135	0.000160368	0.001151176	0.02	Down
mmu00980	Metabolism of xenobiotics by cytochrome P450	19/73	0.000175997	0.001151176	0.02	Down
mmu01240	Biosynthesis of cofactors	74/154	0.000178113	0.001151176	0.04	Down
mmu00730	Thiamine metabolism	5/15	0.000187401	0.001151176	0.02	Down

mmu00020	Citrate cycle (TCA cycle)	30/32	0.00020177	0.001156812	0.01	Down
mmu01200	Carbon metabolism	81/121	0.000404805	0.002175826	0.02	Down
mmu00760	Nicotinate and nicotinamide metabolism	11/41	0.000459649	0.002325283	0.04	Up
mmu00860	Porphyrin and chlorophyll metabolism	19/43	0.000549279	0.002624333	0.04	Up
mmu00360	Phenylalanine metabolism	7/23	0.000744591	0.003370253	0.01	Up
mmu00630	Glyoxylate and dicarboxylate metabolism	20/32	0.000794408	0.003415956	0.02	Down
mmu00480	Glutathione metabolism	28/72	0.001037994	0.004250832	0.02	Down
mmu00061	Fatty acid biosynthesis	12/19	0.00119934	0.004323466	0.04	Up
mmu00052	Galactose metabolism	17/32	0.001212032	0.004323466	0.02	Down
mmu00350	Tyrosine metabolism	12/40	0.001275764	0.004323466	0.02	Down
mmu00900	Terpenoid backbone biosynthesis	8/23	0.001283046	0.004323466	0.01	Down
mmu00140	Steroid hormone biosynthesis	12/92	0.001307094	0.004323466	0.02	Down
mmu00511	Other glycan degradation	11/18	0.001620057	0.005160182	0.03	Down
mmu00520	Amino sugar and nucleotide sugar metabolism	29/51	0.001922509	0.005904848	0.02	Down
mmu00040	Pentose and glucuronate interconversions	9/35	0.002291756	0.006796243	0.02	Down
mmu00620	Pyruvate metabolism	34/44	0.004741112	0.013428366	0.02	Down
mmu00524	Neomycin, kanamycin and gentamicin biosynthesis	3/5	0.004840458	0.013428366	0.02	Down
mmu00053	Ascorbate and aldarate metabolism	9/31	0.005220665	0.013429037	0.01	Down
mmu00830	Retinol metabolism	8/97	0.005279453	0.013429037	0.01	Down
mmu00531	Glycosaminoglycan degradation	10/21	0.005309154	0.013429037	0.02	Down
mmu00450	Selenocompound metabolism	9/17	0.006951355	0.017080471	0.02	Down
mmu00250	Alanine, aspartate and glutamate metabolism	17/39	0.007955263	0.019004239	0.02	Down
mmu01230	Biosynthesis of amino acids	45/79	0.008873164	0.020624111	0.02	Down
mmu01212	Fatty acid metabolism	40/62	0.009336325	0.021129578	0.03	Down
mmu00500	Starch and sucrose metabolism	14/34	0.011170016	0.024631316	0.02	Down
mmu00514	Other types of O-glycan biosynthesis	15/43	0.011876496	0.025349557	0.04	Up
mmu01210	2-Oxocarboxylic acid metabolism	11/20	0.01227639	0.025349557	0.01	Down
mmu00650	Butanoate metabolism	13/28	0.012404185	0.025349557	0.01	Down
mmu00670	One carbon pool by folate	9/19	0.012674778	0.025349557	0.05	Down
mmu00310	Lysine degradation	20/64	0.01401052	0.027384197	0.02	Down

mmu00590	Arachidonic acid metabolism	9/86	0.015253177	0.029150517	0.01	Down
mmu00770	Pantothenate and CoA biosynthesis	8/21	0.016632522	0.031095584	0.02	Down
mmu00592	alpha-Linolenic acid metabolism	3/25	0.017819371	0.032605657	0.03	Up
mmu00780	Biotin metabolism	3/3	0.018650597	0.033415653	0.01	Down
mmu00640	Propanoate metabolism	25/31	0.020182799	0.035173564	0.02	Down
mmu00290	Valine, leucine and isoleucine biosynthesis	2/4	0.02053428	0.035173564	0.02	Down
mmu00920	Sulfur metabolism	7/11	0.021206387	0.035173564	0.02	Down
mmu00062	Fatty acid elongation	15/19	0.021267736	0.035173564	0.02	Down
mmu00604	Glycosphingolipid biosynthesis - ganglio series	5/15	0.022065753	0.035804807	0.02	Down
mmu00563	Glycosylphosphatidylinositol (GPI)-anchor biosynthesis	8/26	0.023553511	0.036186307	0.04	Down
mmu00750	Vitamin B6 metabolism	3/9	0.023553511	0.036186307	0.03	Up
mmu00220	Arginine biosynthesis	7/20	0.024245413	0.036186307	0.02	Down
mmu00270	Cysteine and methionine metabolism	29/53	0.025410276	0.036186307	0.03	Up
mmu00051	Fructose and mannose metabolism	17/36	0.02551991	0.036186307	0.04	Down
mmu00071	Fatty acid degradation	30/52	0.025667032	0.036186307	0.02	Down
mmu00330	Arginine and proline metabolism	23/54	0.025667032	0.036186307	0.02	Down
mmu00561	Glycerolipid metabolism	23/62	0.025667032	0.036186307	0.03	Down
mmu00010	Glycolysis / Gluconeogenesis	40/67	0.050728869	0.068166917	0.02	Down
mmu00030	Pentose phosphate pathway	17/33	0.050728869	0.068166917	0.03	Down
mmu00410	beta-Alanine metabolism	19/32	0.050728869	0.068166917	0.01	Down

Table 3. ROS pathways are transcriptionally upregulated in the adrenal cortex of LPS-treated mice. The pathway analysis of differentially expressed genes was done with the software package EGSEA and queried against the GO Gene Sets repository. Pathways with padj. < 0.05 are shown.

ID	Gene Set	Number of expressed genes	p value	p adj	avg.logfc	Direc-tion
M13446	GO Regulation of reactive oxygen species metabolic process	271/275	3.75E-08	1.26E-06	1.0100	Up
M13580	GO Positive regulation of reactive oxygen species metabolic process	182/186	2.33E-07	6.26E-06	1.0100	Up

M16953	GO Response to reactive oxygen species	300/317	0.003422132	0.009035375	0.8600	Up
M16581	GO Cellular response to reactive oxygen species	173/177	0.002537297	0.009035375	0.7600	Up
M10618	GO Negative regulation of response to reactive oxygen species	24/24	0.0072384	0.010942115	0.7100	Up
M15379	GO Regulation of reactive oxygen species biosynthetic process	145/148	5.90E-05	0.000770609	0.7000	Up
M10827	GO Positive regulation of reactive oxygen species biosynthetic process	120/123	0.000465606	0.00454261	0.7000	Up
M15990	GO Reactive oxygen species metabolic process	163/167	0.008936465	0.012568942	0.6700	Up
M16764	GO Regulation of response to reactive oxygen species	43/43	0.006753207	0.010498628	0.6200	Down
M16007	GO Negative regulation of reactive oxygen species biosynthetic process	23/23	0.016434387	0.020274996	0.6000	Up
M12185	GO Reactive oxygen species biosynthetic process	32/33	0.006483259	0.01024232	0.5700	Down
M10894	GO Negative regulation of reactive oxygen species metabolic process	59/59	0.006538654	0.010287661	0.5500	Up

Table 4. ROS – related protein expression is upregulated in the adrenal cortex of LPS-treated mice. The pathway analysis of differentially expressed proteins was done with the software package EGSEA and queried against the GO Gene Sets repository. Pathways with padj. < 0.05 are shown.

ID	Protein Set	Number of detected proteins	p.value	p.adj	avg.logfc	Direc-tion
M13446	GO REGULATION OF REACTIVE OXYGEN SPECIES METABOLIC PROCESS	62/275	6.30E-06	0.00012401	0.03	Up
M15379	GO REGULATION OF REACTIVE OXYGEN SPECIES BIOSYNTHETIC PROCESS	34/148	9.43E-06	0.00014372	0.03	Up
M13580	GO POSITIVE REGULATION OF REACTIVE OXYGEN SPECIES METABOLIC PROCESS	29/186	1.11E-05	0.00015778	0.03	Up
M10827	GO POSITIVE REGULATION OF REACTIVE OXYGEN SPECIES BIOSYNTHETIC PROCESS	20/123	1.17E-05	0.00016203	0.03	Up
M10894	GO NEGATIVE REGULATION OF REACTIVE OXYGEN SPECIES METABOLIC PROCESS	23/59	5.29E-05	0.00037856	0.05	Down
M16007	GO NEGATIVE REGULATION OF REACTIVE OXYGEN SPECIES BIOSYNTHETIC PROCESS	12/23	0.00014126	0.00073167	0.07	Up
M16581	GO CELLULAR RESPONSE TO REACTIVE OXYGEN SPECIES	50/177	0.00015378	0.00077551	0.03	Down

M15990	GO REACTIVE OXYGEN SPECIES METABOLIC PROCESS	35/167	0.00037436	0.00150479	0.02	Down
M16953	GO RESPONSE TO REACTIVE OXYGEN SPECIES	83/317	0.00076076	0.00262274	0.03	Up
M12185	GO REACTIVE OXYGEN SPECIES BIOSYNTHETIC PROCESS	9/33	0.00192844	0.00545214	0.02	Down

Table 5. Primers for RT-qPCR.

Gene name	**Forward Sequence (5' → 3')**	**Reverse Sequence (5' → 3')**
mouse 18S rRNA	GTTCCGACCATAAACGATGCC	TGGTGGTGCCCTTCCGTCAAT
mouse Idh1	GTGGTGGAGATGCAAGGAGAT	TGGTCATTGGTGGCATCACG
mouse Idh2	GATGGACGGTGACGAGATGAC	GGTCTGGTCACGGTTTGGA
mouse Sdhb	GGACCTCAGCAAAGTCTCCAA	TGCAGATACTGTTGCTTGCC
mouse Sdhc	GCTAAGGAGGAGATGGAGCG	AGAGACCCCTCCACTCAAGG
mouse Star	CTGTCCACCACATTGACCTG	CAGCTATGCAGTGGGAGACA
mouse Cyp11b1	TCACCATGTGCTGAAATCCTTCCA	GGAAGAGAAGAGAGGGCAATGTGT
mouse 3bHsd2	GCGGCTGCTGCACAGGAATAAAG	TCACCAGGCAGCTCCATCCA
mouse Cyp21a1	TGGGGATGCAAGATGTGGTGGT	GGTCGGCCAGCAAAGTCCAC
mouse Cyp11a1	GGATGCTGGAGGAGATCGT	GAAGTCTGGAGGCAGGTTGA
mouse Cd31	TGCAGGAGTCCTTCTCCACT	ACGGTTTGATTCCACTTTGC
mouse Cd45	CCAGTCATGCTACCACAACG	TGGACATCTTTGAGGTCTGCC
mouse Il1r1	TGGAAGTCTTGTGTGCCCTT	TCCGAAGAAGCTCACGTTGT
human 18S	TGCCCTATCAACTTTCGATG	GATGTGGTAGCCGTTTCTCA
human SDHB	CAAGGCTGGAGACAAACCTCA	GGGTGCAAGCTAGAGTGTTG

Figures

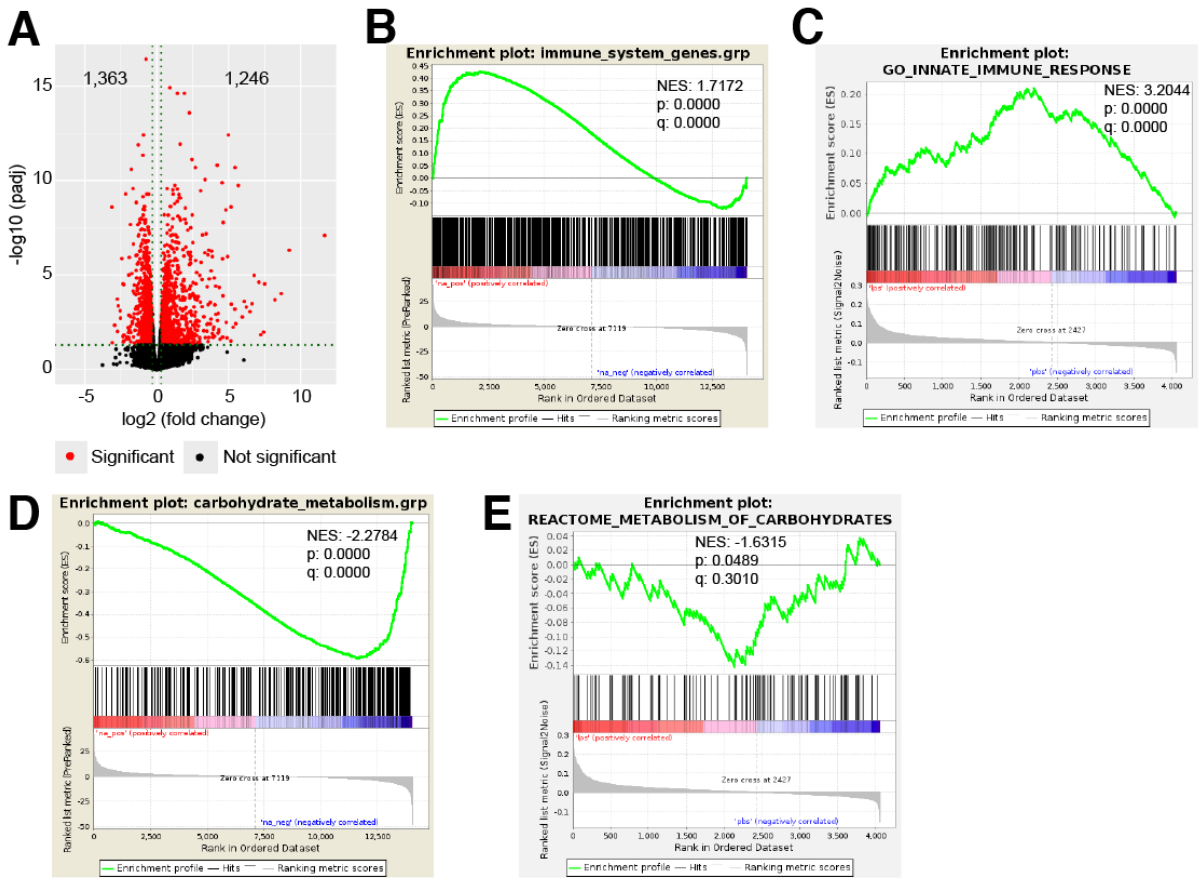

Figure 1. LPS-induced inflammation changes the transcriptional and proteomic profile of the adrenal cortex.

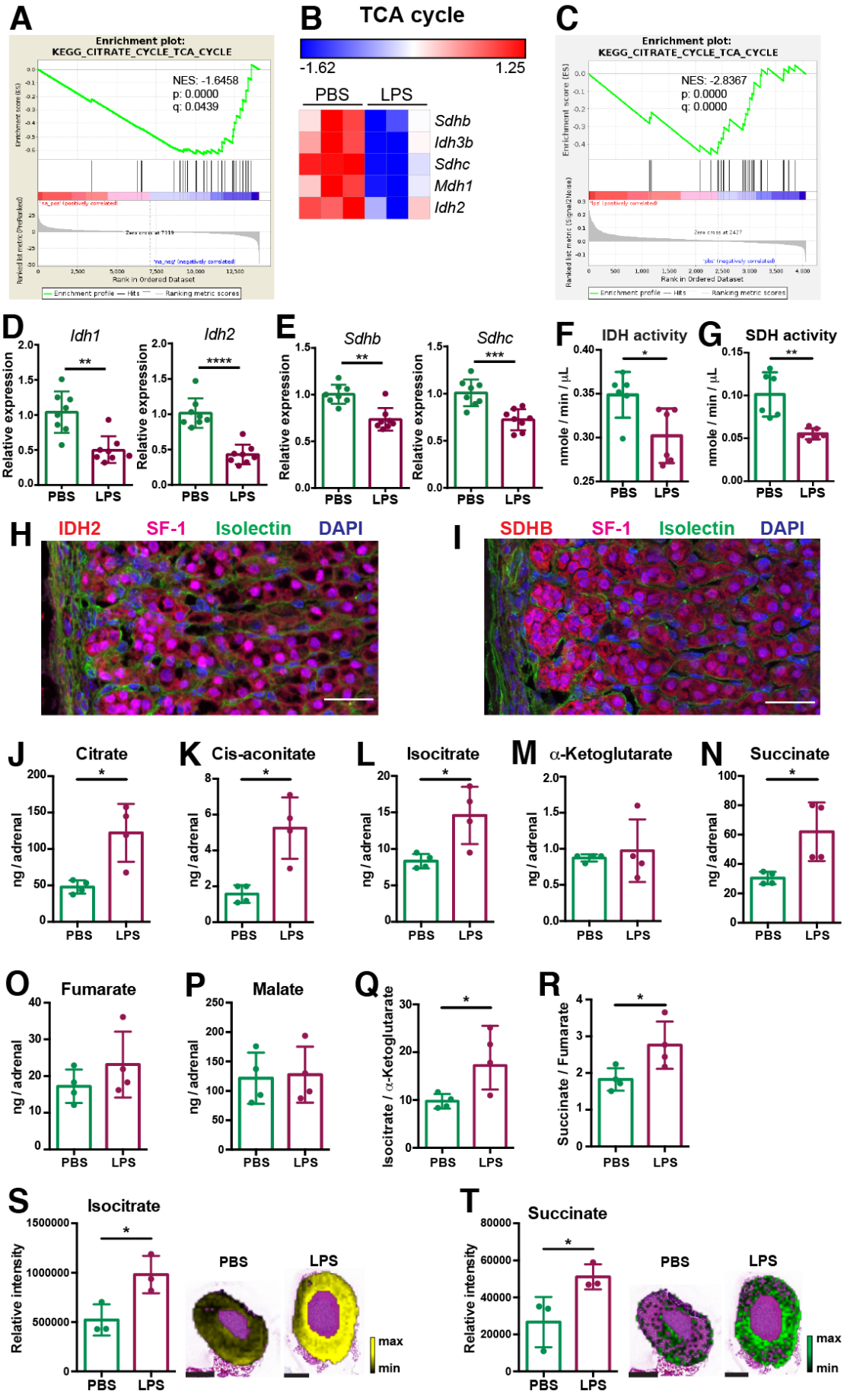

Figure 2. Systemic inflammation disrupts the TCA cycle in the adrenal cortex.

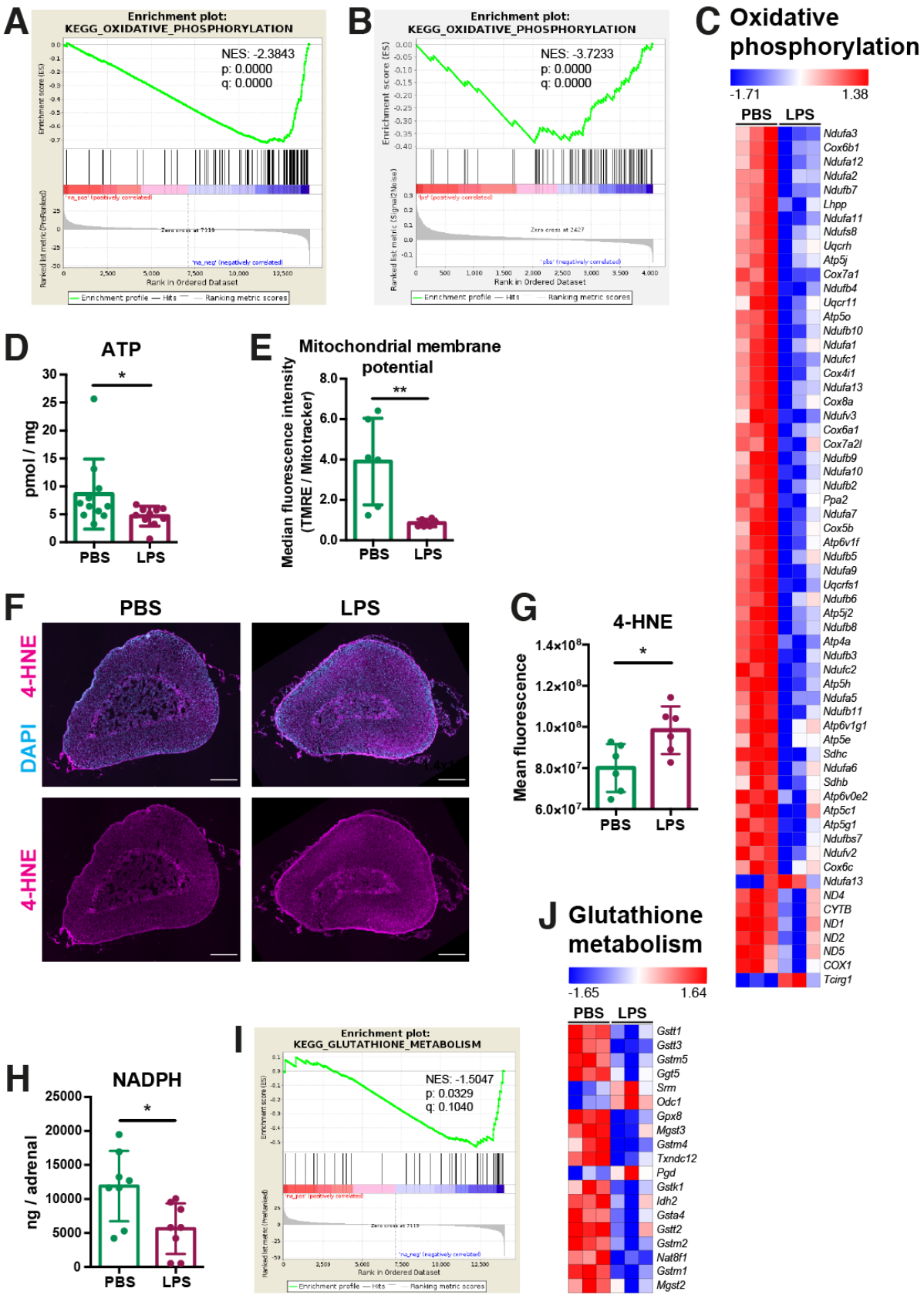

Figure 3. Inflammation downregulates oxidative phosphorylation and increases oxidative stress in the adrenal cortex.

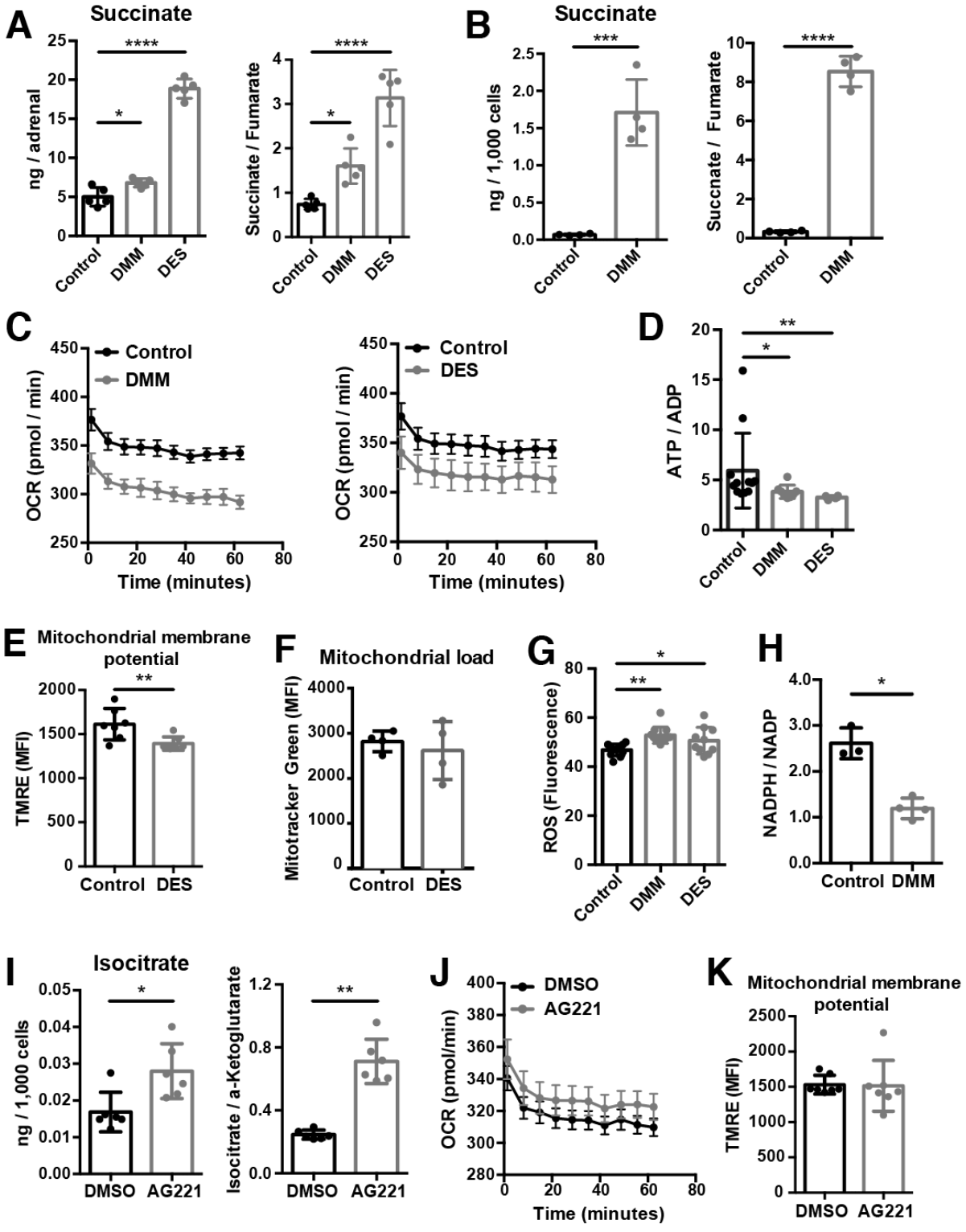

Figure 4. Disruption of succinate dehydrogenase function in adrenocortical cells impairs mitochondrial metabolism and function.

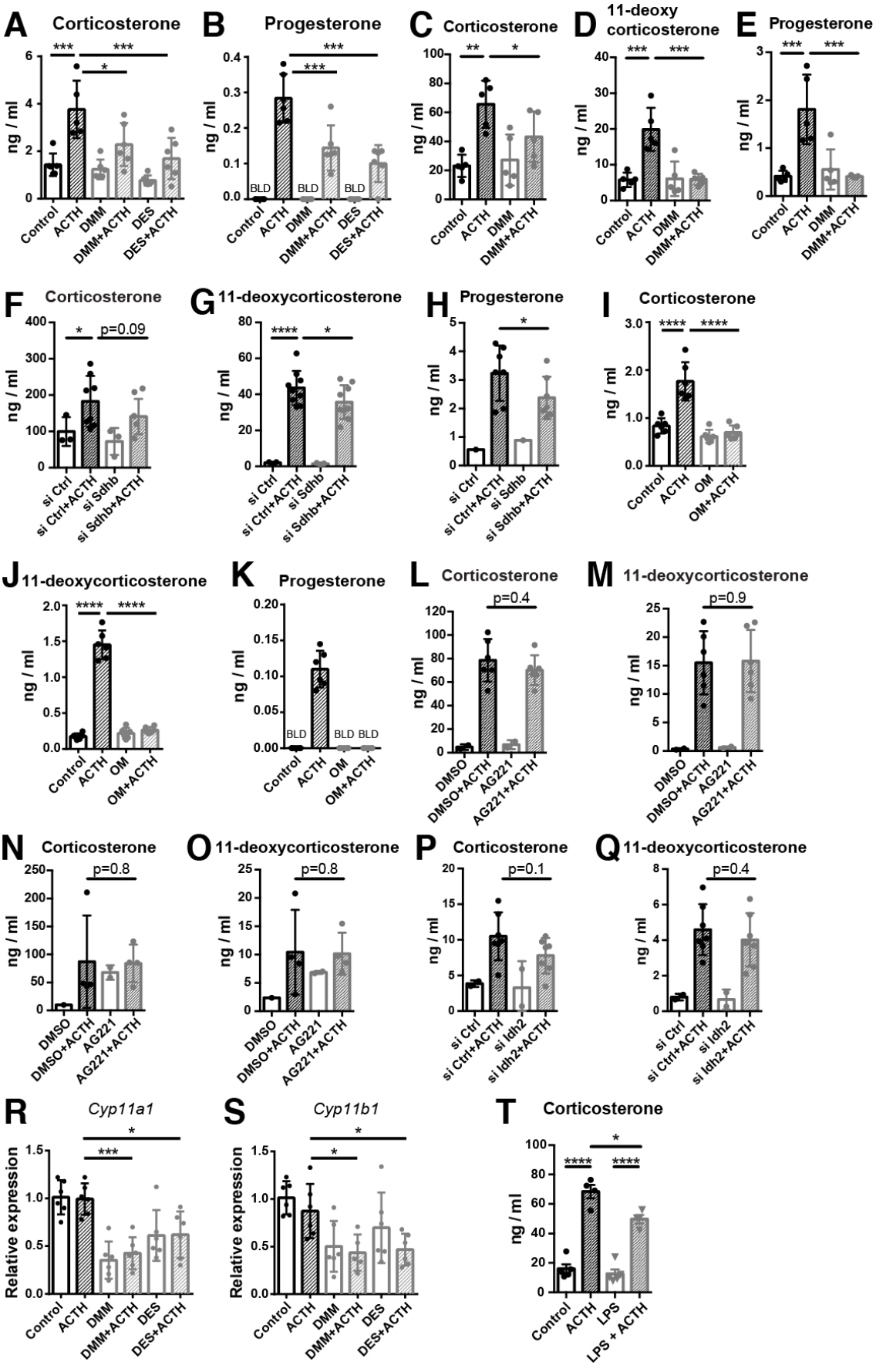

Figure 5. Disruption of succinate dehydrogenase function in adrenocortical cells impairs glucocorticoid production in the mouse adrenal cortex.

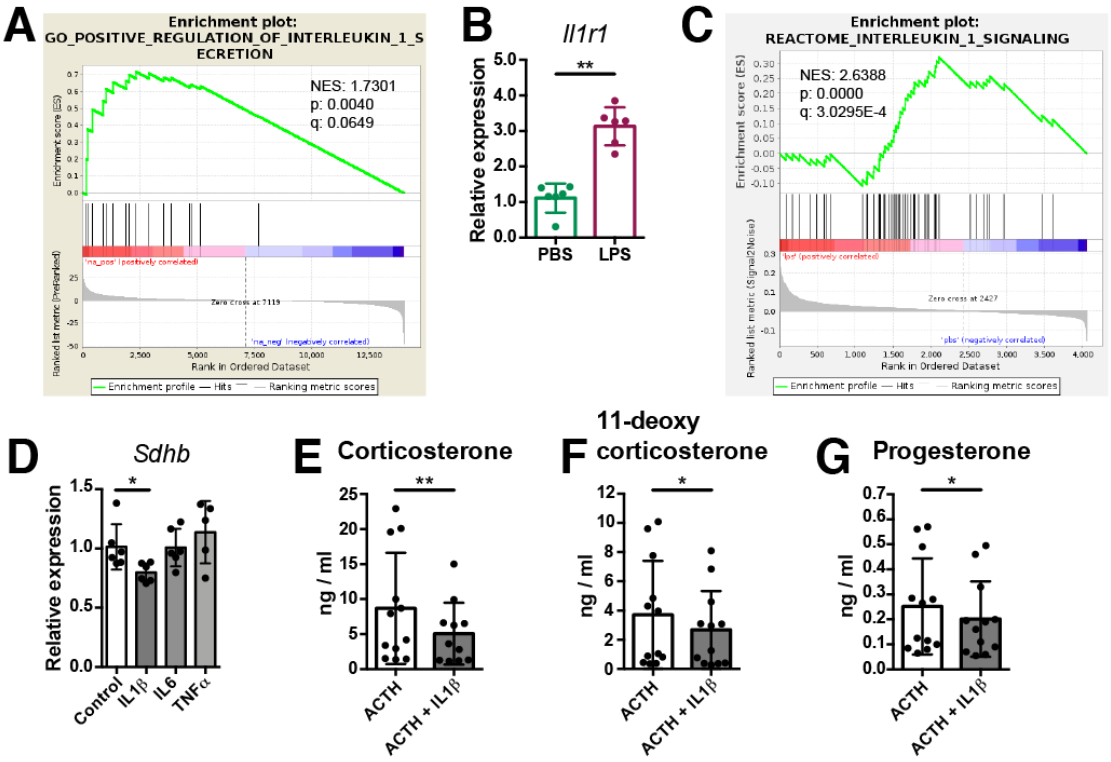

Figure 6. IL1β reduces glucocorticoid synthesis in adrenocortical cells.